

Time variability of ultra fast BAL outflows using SALT: C IV equivalent width analysis [★]

P. Aromal^{1†}, R. Srianand¹, and P. Petitjean²

¹*IUCAA, Postbag 4, Ganeshkind, Pune 411007, India*

²*Institut d’Astrophysique de Paris, Sorbonne Université and CNRS, 98bis boulevard Arago, 75014 Paris, France*

Accepted XXX. Received YYY; in original form ZZZ

ABSTRACT

We study the time variability (over ≤ 7.3 yrs) of ultra fast outflows (UFOs) detected in a sample of 64 C IV broad absorption line (BAL) quasars (with 80 distinct BAL components) monitored using the Southern African Large Telescope. By comparing the properties of the quasar in our sample with those of a control sample of non-BAL quasars we show that the distributions of black hole mass are different and the bolometric luminosities and optical photometric variations of UFO BAL quasars are slightly smaller compared to that of non-BAL quasars. The detection fraction of C IV equivalent width (W) variability ($\sim 95\%$), the fractional variability amplitude ($\frac{\Delta W}{W}$) and the fraction of “highly variable” BAL (i.e., $|\frac{\Delta W}{W}| > 0.67$) components ($\sim 33\%$) are higher in our sample compared to the general BAL population. The scatter in $\frac{\Delta W}{W}$ and the fraction of “highly variable” BALs increase with the time-scale probed. The $\frac{\Delta W}{W}$ distribution is asymmetric at large time scales. We attribute this to the BAL strengthening time scales being shorter than the weakening time scales. The BAL variability amplitude correlates strongly with the BAL properties compared to the quasar properties. BALs with low W , high-velocity, shallow profiles, and low-velocity width tend to show more variability. When multiple BAL components are present a correlated variability is seen between low- and high-velocity components with the latter showing a larger amplitude variations. We find an anti-correlation between the fractional variations in the continuum flux and W . While this suggests photoionization-induced variability, the scatter in continuum flux is much smaller than that of W .

Key words: galaxies:active – quasars: absorption lines – quasars: general

1 INTRODUCTION

In the spectra of 10%–20% of optically selected QSOs, strong absorption features, so-called Broad Absorption Lines (BAL), of Si IV, C IV and N V (occasionally of Fe II and Mg II, Wampler et al. 1995) are observed blueshifted up to 0.2c from the corresponding rest-frame emission lines (Weymann et al. 1991). It has been suggested that the intrinsic BAL fraction, after accounting for dust and other observational biases, could be as high as $\sim 40\%$ (Dai et al. 2008; Allen et al. 2011). Rare examples of QSO spectra exhibiting broad absorption lines redshifted with respect to the emission lines

are also known (e.g., Hall et al. 2013). Based on large velocity widths and blue shifts it is believed that the absorbing gas is related to the central regions of quasars. The BAL fraction among quasars reflects either the covering factor of outflows that prevail in all quasars (e.g., Elvis 2000) or a precise AGN evolutionary phase (e.g., Wang et al. 2013; Chen et al. 2022). Based on the measured properties like blackhole mass (M_{BH}), Eddington ratio (λ_{Edd}) etc., hot dust emission, and overall optical-IR spectral energy distribution (SED), it appears that both BAL and non-BAL QSOs are drawn from the same parent population (Reichard et al. 2003; Rankine et al. 2020; Yi et al. 2020; Temple et al. 2021). While this may favor the first possibility, it does not rule out the BAL being part of an evolutionary sequence. It is also widely believed that these outflows could play an important role in the central black hole growth, the host galaxy evolution (Ostriker et al. 2010; Kormendy & Ho 2013), and the chemical enrichment of the intergalactic medium (Wampler et al.

[★] Based on observations collected at Southern African Large Telescope (SALT; Programme IDs 2015-1-SCI-005, 2018-1-SCI-009, 2019-1-SCI-019 and 2020-1-SCI-011) and the European Organisation for Astronomical Research in the Southern Hemisphere under ESO programme 093.A-0255.

[†] E-mail: aromal@iucaa.in (PA)

1995; Dunn et al. 2010; Capellupo et al. 2012; Borguet et al. 2013).

Very large velocity outflows ($v_{out} \sim 0.1 - 0.2c$) are seen both in the form of X-ray (e.g., Ultra fast outflows (UFOs) studied by Tombesi et al. 2010) and UV (e.g., Extremely high-velocity outflows, EHVOs, studied by Rodríguez Hidalgo et al. 2020) absorption. BAL outflows with such large velocities are interesting as to achieve large terminal velocities, the launching power ($\propto v_{out}^3$) must be very large and the wind must be launched very close to the central engine (see for example, Murray et al. 1995). Hence these outflows that carry large momentum can significantly influence the properties of gas in host galaxies and be part of what is known as AGN feedback (Hopkins & Elvis 2010). Also, the origin and evolution of the UFO BALs can be considerably different from their lower velocity counterparts, hence a study which focuses on absorption as a function of its velocity will provide additional clues on their launching and acceleration mechanism. A similar study done by Tombesi et al. (2013) for X-ray outflows concludes that the X-ray UFOs and the comparatively lower velocity warm absorbers could actually represent parts of a single large-scale stratified outflow observed at different locations from the black hole where the X-ray UFOs are likely launched from the inner accretion disc and the WAs at larger distances, such as the outer disc and/or torus.

In particular, the exact mechanism that can accelerate the absorbing gas to such large velocities is still debated. Line-driven radiative acceleration is generally preferred based on the evidence found through observations of line-locking (e.g., Srianand et al. 2002) and the Ly α ghost signature (e.g., Arav 1996). Also, note that Bowler et al. (2014) found line-locking in both BAL and non-BAL populations with similar frequency suggesting line-driving is important in both populations. Given the high luminosity of the quasar, an extended uniform-density absorber will be too highly ionized to produce C IV absorption out to ~ 1 kpc (Baskin et al. 2014). Therefore it will be very difficult to accelerate the gas through line-driven acceleration as it is expected to be highly ionized. In the framework of the traditional disk-wind model, Murray et al. (1995) suggested that this over-ionization problem can be avoided by introducing a highly ionized gas component (i.e., the so-called shielding gas) located close to the ionizing source that acts as a screen to prevent the high energy photons from heating the gas producing BAL (see also Proga et al. 2000; Higginbottom et al. 2013; Matthews et al. 2016). Such a scenario can also be useful in understanding the X-ray weakness of BAL quasars (Gibson et al. 2009; Stalin et al. 2011). Alternatively, magnetic driving can also explain high velocity and highly ionized gas (de Kool & Begelman 1995).

The validity of a given outflow model and/or constraints on the parameters of models can be obtained using high-resolution spectroscopic observations and/or spectroscopic monitoring with adequate time sampling. While the former can be used to constrain density, covering factor, chemical enrichment, and location of the gas the latter is useful in constraining variability time scales that can be linked to density and or time scales of either the gas ejection event and/or transverse motions. The distance measurement obtained for some of the BALs using fine-structure excitation tend to be very large (see for example, Arav et al. 2018). While large

distances make BAL outflows an important contributor to the AGN feedback, it poses a problem to simulations as distance scales are much smaller in simulations. Time dependence, velocity dependence, and correlated velocity scale of absorption line variability can also provide interesting constraints for the disk wind models. Here we mainly focus on the variability of C IV BALs having high ejection velocities.

The existence of BAL variability has been known for over three decades (e.g., Foltz et al. 1987; Barlow et al. 1992) and surveys of increasing number of objects have become common (Lundgren et al. 2007; Gibson et al. 2008, 2010; Filiz Ak et al. 2012; Capellupo et al. 2011, 2012; Vivek et al. 2014; Filiz Ak et al. 2013; McGraw et al. 2017; Rogerson et al. 2018; Vivek et al. 2018; De Cicco et al. 2018; Aromal et al. 2022). In general, the BAL variability includes extreme optical depth variations like emergence, disappearance, and kinematic shifts. Possible origins of BAL variability are: (i) large variations in the quasar ionizing flux, (ii) changes in the covering factor (f_c) of the outflow with respect to the background source, (iii) the transverse motion of the outflow perpendicular to our line of sight. Detailed investigation of the time variability of BAL profiles can yield tight constraints on the lifetime and the location of the outflow, and provides significant insights on the origin and physical mechanisms driving the flow. If the BALs are formed in the vicinity of the launching region, then the timescale for wind material to cross the region of interest is about 1–10 yr, and this is a reasonable characteristic timescale over which flow structures are expected to change (Capellupo et al. 2013). This is also the characteristic timescale for significant angular rotation of the accretion disk at the wind-launching radius.

For the past several years, we have been carrying out a low-resolution spectroscopic monitoring of a sample of 64 quasars that show C IV BALs with outflow velocities (v_{out}) greater than 15000 km s^{-1} (refer to as UFO BAL in this work) using the Southern African Large Telescope (SALT). Detailed analysis of two of these quasars was presented in our previous papers (Aromal et al. 2021, 2022). In this paper, we focus on the statistical analysis of the full sample. In particular, we study the C IV equivalent width variability of UFO BALs over time scales up to ~ 7.3 yrs. Our main aim is to quantify, the C IV equivalent width variability, its dependence on time-scale, physical parameters of quasar and the BAL absorption profile, emergence/disappearance and acceleration signatures and their correlation to broad emission lines and continuum variability.

This article is arranged as follows. In Section 2 we present our sample of UFO BALs, methods for identifying BAL regions and their variations, and also construct a control sample of non-BAL quasars matched in r-band magnitude and redshift. Section 3 provides details of spectroscopic and photometric data used in this study and compares certain photometric and spectral properties of UFO BALs to that of the quasars in the control sample. Section 4 presents our results on BAL variability and its dependence on time-scale, quasar and BAL properties, properties of C IV emission line and photometric variability nature of the quasars. In section 5, we discuss our main results and their implications. Throughout this paper we use the flat Λ CDM cosmology with $H_0 = 70 \text{ km s}^{-1} \text{ Mpc}^{-1}$ and $\Omega_{m,0} = 0.3$.

2 UFO BAL SAMPLE AND CONTROL SAMPLES

We have constructed a sample of C IV UFO BALs from the SDSS data release 12 quasar population (Pâris et al. 2017) by applying the following criteria. The BAL parameter in the catalog of Pâris et al. (2017) should be set to 1 and the Balnicity index (BI) should be greater than 0 km s^{-1} . The observed maximum outflow velocity at the time of observations should be $v_{\text{outflow, max}} > 15000 \text{ km s}^{-1}$. We restrict our sample to quasars having $z_{\text{em}} > 2.0$ to ensure that C IV (also Si IV in most cases) absorption falls in the optical region and in the most sensitive wavelength range of the spectra in the case of both SDSS and SALT observations. We also restrict our sample to objects with declination $< +10$ deg and magnitude brighter than $m_r = 18.5$ mag. The former is to ensure that the source is accessible to SALT and the latter is to ensure that we get a sufficiently high spectroscopic signal-to-noise ratio (SNR) even if the observing conditions are sub-optimal with SALT.

We end up with a sample of 66 sources. From these sources, we remove 2 sources (namely, J021119.65-042158.2 and J110100.38+092314.30), where wrong identifications of BELs have led to inaccurate redshifts and the correct redshifts are found to be $z_{\text{em}} < 2$. After visual inspection of the spectra, we remove another source, namely J002248.46-044510.3, where the identification of BAL is suspected to be wrong. Hence, we find a total of 63 UFO BAL sources from the SDSS DR12 catalog. We add to this list another UFO BAL source namely J132216.25+052446.3, an interesting BAL quasar we have been monitoring for the past 7 years using SALT. This source is identified as a BAL QSO in the SDSS DR12 BAL quasar sample, but the UFO BAL is absent in the SDSS spectrum and has only emerged during our other observing programme (Aromal et al. 2022). Our final sample consists of 64 UFO BAL quasars which are studied in detail in this paper. The median values of the r-band magnitude and z_{em} are 18.25 and 2.3437 respectively for quasars in our sample. The list of sources, log of observations, and details of spectra obtained at different epochs are given in Table B1 in the online material.

In Table 1 we provide some physical characteristics of the quasars in our sample. Columns 8, 9 and 10 of Table 1 give, respectively, the mass of the central black hole (M_{BH}), the bolometric luminosity (L_{Bol}) and the Eddington ratio (λ_{Edd}). The emission redshift (z_{em} , given in column 2) is taken from Hewett & Wild (2010) (which derives the systemic redshift from the fit of the C III] emission line) whenever available and if not from Pâris et al. (2017).

2.1 BAL identification

We used the publicly available multi-component spectral fitting code PyQSOFIT¹ (Guo et al. 2018) to fit the continuum and broad emission lines (BEL) of all quasar spectra in our sample. We visually inspected each spectrum and identified wavelength ranges devoid of any absorption lines. We then fitted these line-free regions with a power-law + multiple Gaussian (for BELs) model which provided fairly good fits using χ^2 minimization as shown in Fig 1 for a few sources

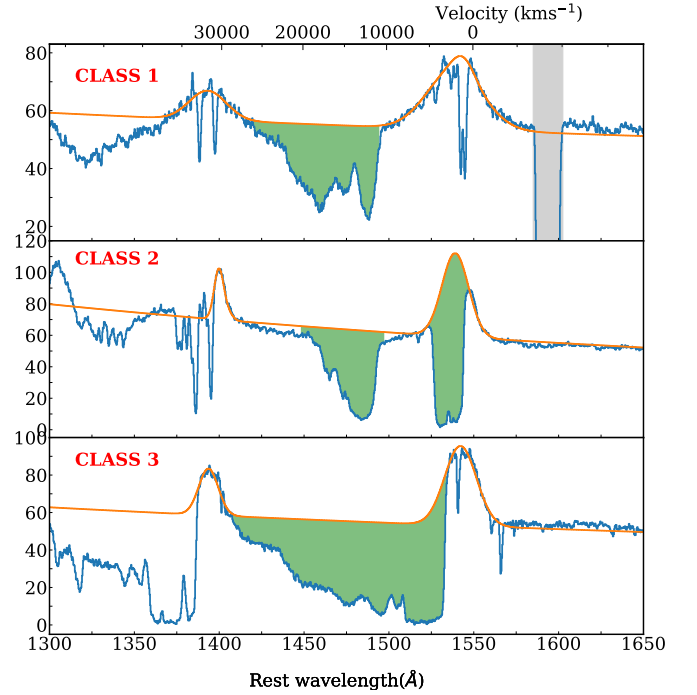


Figure 1. Examples of observed spectra and the best fits to the continuum and broad emission lines are shown in blue and orange respectively. Each panel shows absorption profiles of UFO BALs (green shaded regions) belonging to different classes as defined later in Section 4.6. The rest wavelength (bottom) and velocity (top) scales are defined with respect to z_{em} given in Table 1. The gray-shaded region in the top panel corresponds to the CCD gap in SALT spectra.

in our sample. For sources where C IV BEL is not severely contaminated by absorption lines, we typically needed two Gaussians to fit the line whereas for all other cases, a single Gaussian was used. Similarly, for other prominent BELs in the spectra like Si IV, N V etc., we used single Gaussian to fit the lines. We then identified BAL troughs using the conventional definition given by Weymann et al. (1991) where a BAL is defined as a continuous absorption wider than 2000 km s^{-1} below 90 % of the continuum level. Note that a spectrum can contain several distinct BAL troughs. Here, we searched for C IV BALs in the region between 3,000 to $30,000 \text{ km s}^{-1}$ from the emission redshift. We do not consider BALs beyond $30,000 \text{ km s}^{-1}$ as they could be contaminated by the Si IV absorption from lower velocities. We consider only BALs beyond $3,000 \text{ km s}^{-1}$ to avoid contamination by narrow associated absorption systems (that appear broad due to blending and moderate resolution spectra used here) that are not part of the BAL flow.

For the identification of BAL complexes, we adopt the same method as in Filiz Ak et al. (2013) (refer to their Section 3.2) as this method helps in efficiently quantifying the BAL variability across different spectroscopic epochs. In short, we define the BAL regions for each source after assigning a minimum and maximum velocity associated with these BALs considering all epochs. These velocities (denoted as v_{min} and v_{max}) for each source are listed in columns 5 and 6 of Table 1. After visually inspecting the results, we clearly identify 80 distinct BAL complexes in our UFO BAL sam-

¹ <https://github.com/legolason/PyQSOFit>

Table 1. Details of quasars with UFOs in our sample

QSO	z_{em}	z_{abs}	v_{min} (km s ⁻¹)	v_{max} (km s ⁻¹)	BI (km s ⁻¹)	Class	$\log(M_{\text{BH}})$ (M _⊙)	$\log(L_{\text{Bol}})$ (erg s ⁻¹)	$\log(\lambda_{\text{Edd}})$	Number of epochs	Δt (yr) (min,max)
(1)	(2)	(3)	(4)	(5)	(6)	(7)	(8)	(9)	(10)	(11)	(12)
J0028-0539	2.5584	2.36	10378	25096	4138	1	9.50	46.98	-0.62	3	0.53, 2.44
J0034+0309	2.3329	2.14	10799	26307	4442	1	9.46	46.88	-0.68	4	0.29, 3.18
J0046+0104	2.1492	2.01	10202	19450	4649	2	9.21	47.30	-0.01	13	0.00, 6.64
J0052+0909	2.6625	2.43	10672	30000	8866	1	9.41	47.05	-0.46	3	0.29, 2.67
J0054+0027	2.5142	2.42	4426	11048	1249	2	9.48	47.16	-0.42	8	0.03, 5.96
		2.31	12220	25899	1246	2	9.48	47.16	-0.42	8	0.03, 5.96
J0138+0124	2.5441	2.42	3000	28896	15374	3	9.21	47.19	-0.12	4	0.24, 3.04
J0152+0929	2.1794	2.04	6840	26925	5516	3	9.31	46.93	-0.48	3	0.32, 3.33
J0200-0037	2.1422	1.99	6846	29777	12261	3	9.29	47.11	-0.27	7	0.70, 6.64
J0216+0115	2.2310	2.19	3191	6227	1337	999	8.98	47.02	-0.06	6	0.31, 6.79
		2.02	7538	29943	6501	999	8.98	47.02	-0.06	6	0.31, 6.79
J0220-0812	2.0095	1.86	9509	29709	6129	1	9.70	47.11	-0.69	5	0.35, 7.00
J0224-0528	2.0845	1.91	14234	20623	1473	1	9.85	47.47	-0.48	3	0.34, 3.19
		1.85	22059	27995	455	1	9.85	47.47	-0.48	3	0.34, 3.19
J0229-0034	2.1382	2.03	3083	28332	13129	3	9.39	47.02	-0.48	14	0.00, 2.55
J0242+0049	2.0573	1.88	10573	26859	3059	2	9.91	47.09	-0.93	9	0.02, 6.85
J0244-0108	3.9856	3.68	10283	27536	5335	1	9.96	47.47	-0.59	6	0.11, 4.37
J0814-0004	2.5936	2.37	10636	29162	2830	1	9.62	47.32	-0.40	4	0.28, 4.39
J0817+0717	2.4428	2.33	4641	18133	6032	3	9.30	47.33	-0.06	2	2.63, 2.63
J0831+0354	2.0761	1.95	8823	27670	6475	1	9.41	46.94	-0.57	3	2.67, 6.18
J0837+0521	2.3624	2.31	3000	7547	1647	2	9.60	47.12	-0.58	3	2.62, 5.34
		2.10	22073	28994	1502	2	9.60	47.12	-0.58	3	2.62, 5.34
J0845+0812	2.3545	2.13	15183	27269	3778	1	9.38	47.08	-0.40	3	0.04, 2.44
J0911+0550	2.7933	2.58	12300	21914	1641	1	9.66	47.52	-0.24	3	1.14, 3.48
J0924-0128	2.4461	2.38	4427	7118	1764	2	8.91	47.16	0.14	2	3.15, 3.15
		2.22	9527	28598	4602	2	8.91	47.16	0.14	2	3.15, 3.15
J0932+0237	2.1679	1.96	13042	30000	7982	1	9.50	47.09	-0.51	4	0.27, 6.59
J0951-0157	3.2553	2.97	14909	27271	3953	1	9.73	47.24	-0.59	3	0.26, 2.62
J1006+0119	2.3030	2.16	6674	24194	8743	3	9.39	47.22	-0.27	2	2.97, 2.97
J1007+0304	2.1245	1.92	15770	24885	1986	1	9.44	47.05	-0.49	6	0.30, 6.13
J1054+0150	2.2366	2.08	13434	17152	1978	1	9.43	46.85	-0.68	4	0.30, 6.14
		2.01	19284	23542	784	1	9.43	46.85	-0.68	4	0.30, 6.14
J1110-0140	2.8192	2.63	8252	24514	6785	1	9.80	47.29	-0.61	3	0.00, 2.88
J1116+0808	3.2429	2.97	16170	24210	663	1	9.29	47.40	0.01	2	2.04, 2.04
J1135-0240	2.4611	2.23	15141	25096	1281	1	9.51	47.05	-0.55	3	0.28, 3.47
J1143+0912	2.3253	2.20	5665	16556	3775	3	9.32	46.92	-0.49	2	2.69, 2.69
J1156+0856	2.1077	1.94	6919	30000	12496	3	8.92	46.75	-0.27	3	2.84, 6.13
J1205+0134	2.1523	1.96	12909	29458	6180	1	9.57	47.09	-0.59	5	0.32, 6.28
J1208+0355	2.0210	1.95	4995	9738	1286	2	9.40	46.88	-0.62	3	2.95, 6.23
		1.82	12972	26326	2808	2	9.40	46.88	-0.62	3	2.95, 6.23
J1215-0034	2.6987	2.54	4151	22790	6568	3	9.94	47.64	-0.40	3	2.46, 5.63
J1301+0314	2.1115	1.91	16175	25380	1656	1	9.58	47.05	-0.63	3	3.22, 6.75
J1317+0100	2.6961	2.59	3816	18015	5987	3	9.17	47.32	0.05	6	0.01, 6.01
		2.45	19596	25568	427	3	9.17	47.32	0.05	6	0.01, 6.01
J1331+0042	2.4341	2.35	6555	9453	498	2	9.37	47.09	-0.38	4	0.01, 3.16
		2.27	11383	16893	468	2	9.37	47.09	-0.38	4	0.01, 3.16
J1341-0115	2.7682	2.55	8502	25835	7132	1	9.72	47.24	-0.59	3	2.33, 5.02
J1343+0351	2.8686	2.68	12032	19532	2192	1	9.92	47.23	-0.79	3	0.25, 2.81
J1350+0843	2.6157	2.44	13629	17632	953	1	9.72	47.30	-0.52	3	0.25, 2.77
J1357+0055	2.0081	1.80	11851	30000	2757	1	9.27	47.32	-0.05	4	0.27, 7.26
J1359+0310	2.6778	2.52	8662	19833	4439	1	9.49	47.28	-0.31	2	2.70, 2.70
J1400+0507	2.3015	2.16	7038	25561	7335	3	9.34	47.01	-0.43	3	0.29, 3.04
J1405+0229	2.8266	2.67	6487	24861	7057	3	9.43	47.25	-0.28	4	0.25, 5.52
J1424+0441	2.2762	2.05	11006	28320	2923	1	9.44	47.12	-0.42	4	0.29, 3.39
J1445-0023	2.2296	2.05	7822	27489	8866	3	9.68	47.40	-0.39	4	0.02, 4.04
J1452+0932	2.4607	2.29	5694	28047	8540	3	9.40	47.24	-0.26	4	0.31, 4.65
J1500+0033	2.4394	2.23	9914	27649	4574	1	9.88	47.27	-0.70	6	0.30, 6.22
J1547+0606	2.0188	1.95	5432	9467	2587	2	9.64	47.27	-0.48	3	2.31, 5.61
		1.87	9984	24909	7467	2	9.64	47.27	-0.48	3	2.31, 5.61
J1606+0718	2.0766	1.99	3835	22135	6819	3	9.46	46.90	-0.66	4	0.34, 5.24
J1606+0746	2.3687	2.20	8414	23723	2005	1	9.72	47.08	-0.74	3	0.29, 2.74
J1609+0526	2.3802	2.27	4115	26115	9608	3	9.29	47.10	-0.29	4	0.28, 4.07

Table 1. Continued

QSO	z_{em}	z_{abs}	v_{min} (km s^{-1})	v_{max} (km s^{-1})	BI (km s^{-1})	Class	$\log(M_{\text{BH}})$ (M_{\odot})	$\log(L_{\text{bol}})$ (erg s^{-1})	$\log(\lambda_{\text{Edd}})$	Number of epochs	Δt (yr) (min,max)
(1)	(2)	(3)	(4)	(5)	(6)	(7)	(8)	(9)	(10)	(11)	(12)
J1621+0758	2.1394	1.98	12355	19811	1016	1	9.58	47.10	-0.58	9	0.02, 5.46
J2126-0211	2.4629	2.23	12298	26593	2717	1	9.33	47.18	-0.25	4	0.28, 3.03
J2130+0115	2.5275	2.26	9697	30000	5839	1	9.62	47.54	-0.18	9	0.00, 4.99
J2137+0844	2.1893	2.12	4314	9046	3094	2	9.32	47.13	-0.28	5	0.01, 3.68
		2.05	10082	23576	4260	2	9.32	47.13	-0.28	5	0.01, 3.68
J2209-0126	2.4227	2.27	5076	30000	12293	3	9.48	47.15	-0.43	5	0.00, 2.84
J2221-0103	2.6754	2.44	9723	29032	5237	1	9.94	47.49	-0.55	6	0.02, 4.77
J2239-0047	2.2200	2.01	14375	25370	1456	1	9.68	47.13	-0.64	6	0.24, 6.18
J2256+0105	2.2680	2.21	3000	8535	2893	2	9.37	47.06	-0.41	5	0.00, 6.07
		2.05	15840	26759	2161	2	9.37	47.06	-0.41	5	0.00, 6.07
J2310+0746	2.3109	2.23	6302	9269	1584	2	9.35	46.95	-0.50	4	0.28, 2.95
		2.19	10000	13108	540	2	9.35	46.95	-0.50	4	0.28, 2.95
		2.08	14232	29382	2197	2	9.35	46.95	-0.50	4	0.28, 2.95
J2352+0105	2.1513	1.92	14600	29706	2182	2	9.70	47.31	-0.49	8	0.03, 6.93
J2355-0357	2.4448	2.26	11721	28163	1513	1	9.76	47.03	-0.83	3	0.27, 2.26
J1322+0524	2.0498	1.97	5680	9830	2116	2	9.75	47.01	-0.84	12	0.00, 6.61
		1.93	10731	13059	288	2	9.75	47.01	-0.84	12	0.00, 6.61
		1.85	15600	26632	2003	2	9.75	47.01	-0.84	9	0.00, 2.28

Column 3 : The absorption redshift of the BAL calculated using the optical depth weighted velocity centroid; Columns 4, 5 and 6 : The minimum velocity (v_{min}), maximum velocity (v_{max}) and balnicity index (BI) of the identified BAL region respectively; Column 7 : The class in which the source belongs according to the shape of the BAL profile as mentioned in Section 4.6. The BAL that could not be fitted into the classification scheme is indicated with ‘999’; Columns 8, 9 and 10 : The estimated quasar properties black hole mass (M_{BH}), bolometric luminosity (L_{bol}) and Eddington luminosity (λ_{Edd}) respectively; Column 11 : The total number of spectroscopic epochs for the source; Column 12 : The minimum and maximum rest-frame time separation between two spectroscopic epochs for the source.

ple. The redshifts of individual BAL complexes and the minimum and maximum velocity spanned by them are provided in columns 3, 4 and 5 respectively in Table 1. The measured maximum Balnicity Index (BI) for individual BAL components are provided in column 6 of the same table.

2.2 BAL variations

Once the BAL troughs were identified, we estimated different C IV BAL properties such as equivalent width (W) and the maximum depth of the BAL (d_{BAL}). The BAL properties at different epochs including W , d_{BAL} etc. are given in Table B2 in the online material. Using the equivalent width as a measure of the strength of the BAL, we quantified the BAL variability by calculating the variations and the fractional variations in W as defined below (see also Filiz Ak et al. 2013) :

$$\Delta W = W_2 - W_1, \quad \sigma_{\Delta W} = \sqrt{\sigma_{W_1}^2 + \sigma_{W_2}^2} \quad (1)$$

$$\frac{\Delta W}{W} = \frac{W_2 - W_1}{(W_1 + W_2) \times 0.5} \quad (2)$$

$$\sigma_{\frac{\Delta W}{W}} = \frac{4 \times (W_1 \sigma_{W_2} + W_2 \sigma_{W_1})}{(W_1 + W_2)^2} \quad (3)$$

where W_1 and W_2 are equivalent widths measured at t_1 and t_2 respectively with $t_1 < t_2$. Thus an increase (or decrease) of W with time results in a positive (or negative) ΔW . Based on the above equation, variations in equivalent width by

a factor of 2 and 3 will correspond to $\Delta W/W$ of 0.67 and 1.0 respectively. An emerging (disappearing) absorption will also correspond to a $\Delta W/W$ of +2 (respectively -2). $\sigma_{\Delta W}$ and $\sigma_{\Delta W/W}$ are errors in ΔW and $\frac{\Delta W}{W}$ respectively.

2.3 Control sample

For comparing different physical properties of UFO BAL quasars in our sample with that of non-BAL quasars, we made a control sample of non-BAL quasars having similar emission redshift ($\Delta z_{\text{em}} \leq 0.2$) and r-band magnitude ($\Delta m_r \leq 0.3$ mag) distributions. For Non-BAL quasars, we selected sources that are included in both SDSS DR7 (Shen et al. 2011) and SDSS DR12 catalogs since Shen et al. (2011) provides several quasar parameters such as black-hole mass (M_{BH}), bolometric luminosity of the quasar (L_{bol}) and Eddington ratio (λ_{Edd}). Hence, we build a sample of 320 non-BAL sources (i.e., 5 non-BAL quasars for each quasar in our UFO sample) following the above criteria. For these objects, we used the parameters provided by Shen et al. (2011) and for the UFO BAL sample, we derived the corresponding quantities from the results of the fits performed with PYQSOFIT and listed them in columns 8-10 of Table 1. Details of how we measure these quantities are provided in the Appendix-A.

Yi et al. (2020) reported a correlation between λ_{Edd} and M_{BH} for their high- z (i.e., $3 \leq z \leq 5$) BAL as well as non-BAL comparison samples. However, the correlation is found to be only tentative in the case of the BAL sample. They attribute this possible difference to the presence of substantial outflows in BAL QSOs as testified by large blueshift in

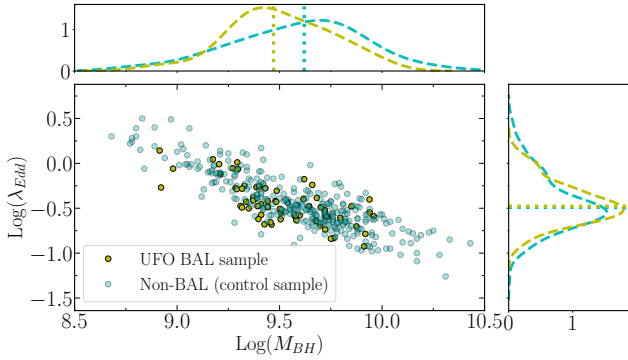


Figure 2. M_{BH} vs. λ_{Edd} for the UFO BAL (yellow points and curves) and non-BAL control sample (green points and curves). A strong anti-correlation is evident for both samples. *Top and right-hand side panels:* PDFs of M_{BH} and λ_{Edd} respectively for the two samples. Dashed lines indicate the median values.

the C IV emission lines. In Fig. 2, we plot M_{BH} vs. λ_{Edd} for our UFO sample as well as for the non-BAL control sample. A strong anti-correlation is apparent in this figure. Visually, the UFO BAL sample traces the same region spanned by the data from the control sample. The Spearman’s coefficients are found to be $r = -0.68$ and $r = -0.82$ for UFO BAL and non-BAL samples respectively. In both cases, the p-values are $< 10^{-3}$ indicating the correlation to be significant.

In the top panel of Fig. 2, we compare the probability distribution function (PDF) for M_{BH} between the UFO BAL and non-BAL control samples. These PDFs were estimated using a non-parametric kernel density estimation (KDE, Silverman 1986) for a fixed bandwidth Gaussian kernel. The median M_{BH} for the UFO BAL and control samples are $10^{9.47}M_{\odot}$ and $10^{9.62}M_{\odot}$ respectively. The KS test confirms the M_{BH} distribution in the two samples to be significantly different with a p-value of 6×10^{-3} . This difference comes from the fact that there is a clear lack of objects with $\log M_{BH} \geq 10.0$ (alternatively quasars with FWHM of C IV BEL more than $10,000 \text{ km s}^{-1}$) and an excess of objects with $\log M_{BH} \sim 9.3$ in our UFO BAL sample. The lack of objects with large M_{BH} (or FWHM of the C IV BEL) may be attributed to the presence of absorption features biasing our Gaussian fits towards lower values.

In the right panel of Fig. 2 we compare the λ_{Edd} PDFs of the UFO BAL and non-BAL control samples. We find the distribution of λ_{Edd} to be similar for both samples. The KS-test also confirms the same with a p-value of 0.60. This lack of difference between the UFO BAL and non-BAL samples is consistent with the finding of Yi et al. (2020), for their high- z ($3 \leq z \leq 5$) BAL QSO sample where the M_{BH} measurements are based on rest-frame optical emission lines. Interestingly, we notice that for a given M_{BH} the λ_{Edd} values observed in our UFO BAL and control samples are lower than that found for the sample of Yi et al. (2020). Two main differences are (i) QSOs in the sample of Yi et al. (2020) are from higher redshifts and (ii) their M_{BH} measurements are based on rest-frame optical lines that are more reliable compared to C IV emission line used in our study.

As a consequence of the above results we find the distributions of Bolometric luminosity are different for non-BAL and the UFO BAL sample (i.e., a p-value of 2.8×10^{-4} for the KS test). This is surprising as we have matched the r-

band magnitudes while constructing the control sample. As the bolometric luminosity is obtained using the rest frame 1350\AA continuum luminosity, the above result suggests a possible difference in the colour distribution of the non-BAL and UFO BAL sub-samples. This may indicate a redder distribution of color for the UFO BAL sample which is consistent with the general understanding that BAL quasars are redder on average than non-BAL quasars (Brotherton et al. 2001; Reichard et al. 2003). However, we do find the median Bolometric luminosity to be similar i.e., $10^{47.22} \text{ erg s}^{-1}$ for the non-BAL control sample and $10^{47.13} \text{ erg s}^{-1}$ for the UFO BAL sample.

3 DETAILS OF OBSERVATIONS AND DATA USED IN THIS STUDY

For the detailed analysis presented in this work, we have used available spectra from the Sloan Digital Sky Survey-I/II (SDSS), Baryon Oscillation Spectroscopic Survey (BOSS) and supplemented them with spectra from our own ongoing spectroscopic monitoring using the Southern African Large Telescope (SALT) (Buckley et al. 2005).

For the SALT observations, we used the Robert Stobie Spectrograph (RSS, Burgh et al. 2003; Kobulnicky et al. 2003) in the long-slit mode with a $1.5''$ wide slit and the PG0900 grating. This combination gives a typical spectral resolution of $\sim 300 \text{ km s}^{-1}$. For each SALT/RSS observation, the GR angle was chosen such that the CCD gaps do not fall in the expected wavelength range of the broad absorption lines. In cases where this was not possible, we tried to observe the target with different GR angles to cover the full wavelength range without any gap. A detailed log of observations for all the objects in our sample is provided in Table B1. In the case of J1621+0758, we also have NTT/ESO observations taken in the year 2014 (details of which can be seen in, Aromal et al. 2021) We have, in total 375 spectra out of which 211 spectra are taken from SDSS and 164 spectra from our SALT observations.

For our SALT observations, the preliminary processing of raw CCD frames were carried out using the SALT data reduction pipeline (Crawford et al. 2010). We used the standard IRAF² procedures to reduce the resulting 2D spectra. Flat-field corrections and cosmic ray zapping were applied to all science frames. We extracted the one-dimensional quasar spectrum from the background subtracted 2D science frames from each epoch using the IRAF task ‘‘apall’’. Wavelength calibration was performed using different standard lamp spectra like Ar, ThAr, HgAr and Xe. In addition, skylines from the wavelength calibrated spectrum were matched with the sky line atlas provided by SALT and, if needed, corrections were applied to increase the wavelength accuracy. Similarly, flux calibration was performed using standard reference stars observed close to our observing nights. We performed continuum fitting to our SALT spectra using the same method described above in Section 2.1.

One of the most important aspects of our study is to

² IRAF is distributed by the National Optical Astronomy Observatories, which are operated by the Association of Universities for Research in Astronomy, Inc., under co-operative agreement with the National Science Foundation.

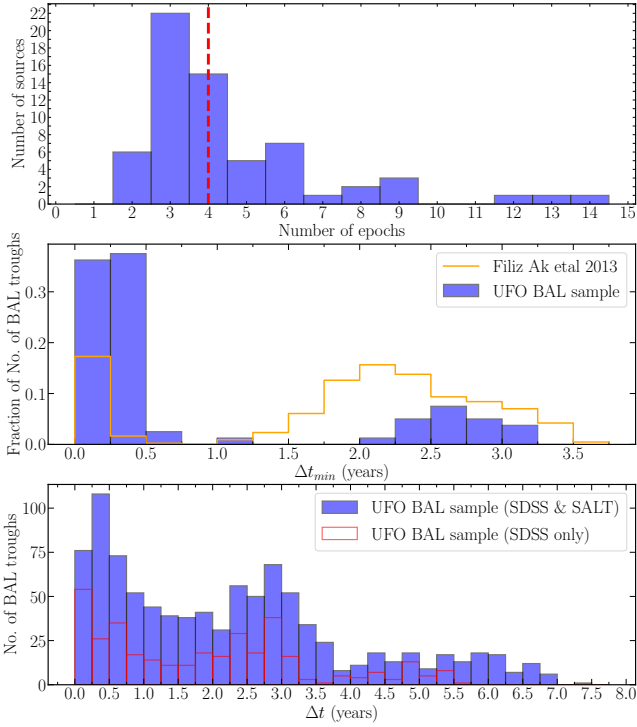


Figure 3. *Top panel:* Distribution of total number of epochs (combining both SDSS and SALT observations) probed for each UFO BAL (blue histogram) with the median of the distribution marked with a red dashed line. *Middle panel:* Distribution of minimum sampled rest-frame time scales, Δt_{min} , for the UFO sample (blue histogram) along with the same distribution for the SDSS sample studied by Filiz Ak et al. (2013) (orange histogram). *Bottom panel:* Time-scales probed by all possible combinations of SDSS and SALT epochs (blue) and only SDSS epochs (red) for each individual source in the sample.

probe both the short- and long- time scale variability of the UFO BAL sample. Our SALT observations, in addition to the SDSS epochs, have brought great improvement to the time-sampling of these UFO BAL sources as demonstrated in Fig 3. The top panel shows the distribution of the total number of spectroscopic epochs for each source with a median value of 4. For 62 out of 64 sources, at least one epoch was added by SALT observations. The middle panel shows the fraction of objects in different minimum sampled rest-frame time scale (Δt_{min}). It can be seen that roughly 70 % of the sources have a minimum separation between the spectroscopic epochs less than 0.5 yr. This is mostly because of the multiple SALT observations performed within a rest frame year which is crucial for characterizing the short-time scale variability. This is a great improvement compared to the study by Filiz Ak et al. (2013) which had only $\sim 20\%$ of such sources (orange histogram in the figure). The bottom panel of Fig 3 shows the histogram of all possible time-scales as probed by both SALT and SDSS (blue) and SDSS alone (red). Again this clearly shows the improvement brought by SALT epochs at different time-scales including $\Delta t > 5.5$ yr.

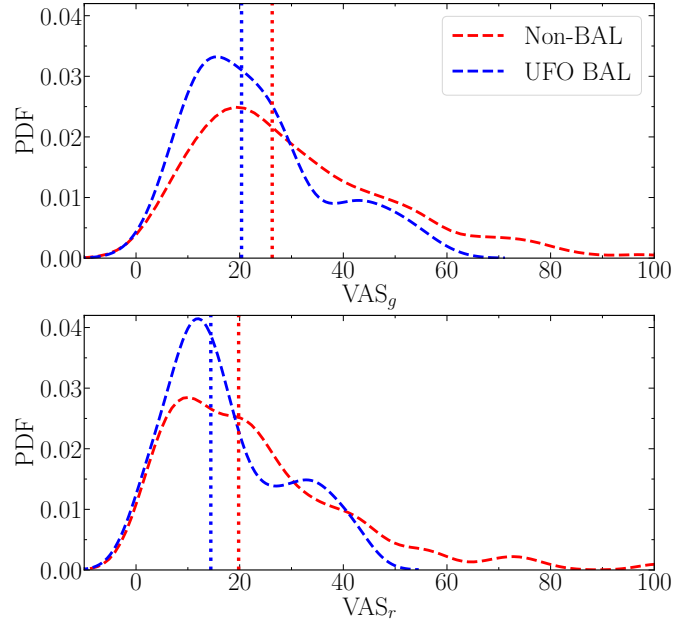


Figure 4. Comparison of variability amplitude strength (VAS) between non-BAL (red) and UFO BAL (blue) samples. Results for the g- and r-bands (VAS_g and VAS_r respectively) are shown in the top and bottom panels respectively. Vertical dashed lines indicate the median values.

3.1 Photometric variability

As in Aromal et al. (2022), we look for correlations between the absorption line variability and the continuum variability using available broad-band photometric light curves. We have obtained publicly available photometric light curves of almost all the UFO BAL sources from the Panoramic Survey Telescope and Rapid Response System (Pan-STARRS; Chambers et al. 2016), the Palomar Transient Factory (PTF; Law et al. 2009) and the Zwicky Transient Facility (ZTF; Bellm et al. 2019a,b) surveys. Pan-STARRS provides photometric data of quasars in five broad band filters, i.e., g, r, i, z and y whereas ZTF gives the same for the g, r and i bands. While PTF and Pan-STARRS provide sparsely sampled light curves ZTF provides much better sampling since the year 2018 (i.e., $MJD \geq 58200$) for all the sources in our UFO BAL QSO sample.

We also obtained all the available ZTF photometric measurements for all quasars in the “non-BAL” control sample. From the ZTF light curves, we first estimate the variability amplitude (σ_{rms}^2) and its error (S_D^2) using the normalized excess variance method described in Vaughan et al. (2003). The variability amplitude strength (VAS) is then defined as $VAS = \sigma_{rms}^2 / S_D^2$. We show the distributions of VAS in g- and r-bands for the two samples in Fig 4. It is interesting to note (from the indicated median values) that the VAS distribution measured for the g-band is wider compared to that of the r-band. This indicates larger amplitude variations at lower wavelengths for quasars in both samples. We also notice that in both the bands the VAS for the UFO BAL sample is smaller than that of the control sample. The KS-test confirms this with a p-value of < 0.1 . Therefore, purely based on optical photometric variability we do not find the

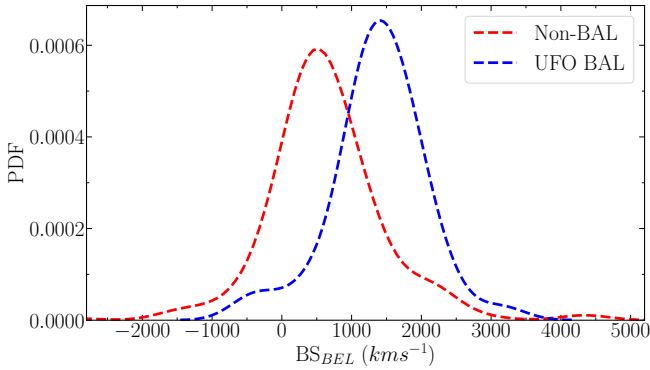


Figure 5. Comparison between C IV BEL blue-shifts in spectra from the non-BAL (blue) and UFO QSO BAL (orange) samples.

quasars in our UFO BAL sample to be more variable compared to the general population of quasars.

3.2 Properties of the C IV emission line

In this section, we mainly focus on the C IV BEL properties of the UFO BALs compared to that of the non-BAL control sample. We recognize that the BEL of UFO quasars may be affected by strong BALs close to the emission redshift. Therefore, we only consider sources having no BALs at velocities less than 6000 km s^{-1} with respect to z_{em} . We also visually inspected the double gaussian fits to the C IV BEL profiles in order to check and remove certain epochs that are severely affected by either narrow absorption lines or CCD gaps in the case of SALT epochs. Thus, we made a sub-sample of 41 sources satisfying the above criteria to compare the emission line properties and study the relationship between UFO BAL and BEL properties.

We estimate two quantities namely, the equivalent width (W_{BEL}) of the emission line and its blueshift (BS_{BEL}) for the C IV BEL. We follow the method by Rankine et al. (2020) in order to calculate BS_{BEL} , i.e.,

$$BS_{\text{BEL}} = c \times (\lambda_r - \lambda_{\text{half}}) / \lambda_r \quad (4)$$

where c is the velocity of light, λ_r is the rest-frame wavelength of the emission line, 1549.48 \AA for the CIV doublet and λ_{half} is the wavelength which bisects the cumulative total line flux.

As shown in Fig 5, we confirm the findings by Rankine et al. (2020) that C IV BELs in sources with BALs reaching high velocities such as our UFO BAL sample tend to show more blue-shifted emission compared to the same of its non-BAL counterparts. But, it is good to keep in mind that the emission-line outflow and physical properties of BAL and non-BAL quasars overlap, hence demonstrating that (high-ionization) BALs and non-BALs represent different views of the same underlying quasar population.

4 RESULTS ON BAL VARIABILITY

4.1 Frequency of BAL variability

Following Filiz Ak et al. (2013), we identify the variable BALs when the C IV BAL equivalent width variation are

$> 3\sigma$ significance level. Using all possible pairs of epochs for each object, we find that $95.3_{-12}^{+14}\%$ of UFO BAL QSOs in our sample show at least one variable trough. Among the 80 UFO BALs identified in Table 1, $95_{-11}^{+12}\%$ of them show $> 3\sigma$ variability. This confirms that $\sim 95\%$ of UFO BAL quasars (and UFO BAL components) in our sample show significant variability at least once between possible pairs of epochs probed. Our results are consistent with that of Gibson et al. (2008) who have found 12/13 of the BALs in their sample to show significant equivalent width variability over 3-6 yrs.

However, smaller variability fractions have also been reported in the literature. Only 11/32 BAL trough in the sample of Lundgren et al. (2007) show more than 3σ equivalent width variability over a time-scale of ≤ 102 days. In their sample of 24 bright BAL quasars Capellupo et al. (2011) have found that 39% and 65% were varied in the short-term (i.e., 4-9 months) and long-term (i.e., 3.8-7.7 yr), respectively. Filiz Ak et al. (2013) have found that 62.2% of BAL quasars and 57.9% of the BAL trough in their sample show significant C IV equivalent width variation when they considered a pair with the shortest time interval for each quasar. The shortest time interval varies for each source due to the non-uniform SDSS observations and ranges from as small as 5.9 hr (10^{-3} yrs) to 3.7 yr with a median of 2.1 yr. If we apply to our sample the same criteria as Filiz Ak et al. (2013), i.e., consider only the pair with the shortest time-scale for each object (see last column in Table 1), we get $\sim 70\%$ of UFO BAL QSOs and UFO BAL components to show variability. We also consider the epoch pairs with the longest time separation (i.e., Δt in the range 2.0–7.3 yr) for each object and found that $\sim 89\%$ and $\sim 87\%$ of UFO BAL QSOs and UFO BAL components show variability respectively. Recall the shortest time intervals probed in our sample (see the middle panel in Fig. 3) are shorter than that of Filiz Ak et al. (2013). As the variability amplitudes are larger for longer time scales (see below), this may indicate that our UFO BALs are showing more variability compared to the general population of BAL quasars at all time scales (section 4.4 provides further discussions on this).

Hemler et al. (2019), studied the very short time-scale (< 10 quasar rest frame days) BAL variability towards 27 BAL QSOs observed as a part of reverberation mapping studies with a median of 58 spectral epochs per quasar. Using all possible combinations of epochs and the C IV equivalent widths given in Table 4 of Hemler et al. (2019), we find that the variable fraction of sources is 96% and the variable fraction of BALs is 92%. This is consistent with what we find in our sample.

To quantify the fraction of variable objects we consider three time bins corresponding to short (0.0-0.5 yrs), intermediate (0.5-2.0 yrs) and long (> 2.0 yrs) time-scales. In the three bins, the percentage of variable sources are $89_{-17}^{+16}\%$, $100_{-17}^{+21}\%$ and $94_{-12}^{+14}\%$ and the percentage of variable BALs are $84_{-12}^{+14}\%$, $97_{-15}^{+18}\%$ and $94_{-10}^{+12}\%$. In the case of the Hemler et al. (2019) observations, we find that the variable fraction of sources are 0.96 and 0.94 and the variable fraction of BALs are 0.92 and 0.90 for the short and intermediate time bins respectively. Thus it appears that, with a suffi-

³ The errors are calculated using Poisson statistics as discussed in Gehrels (1986).

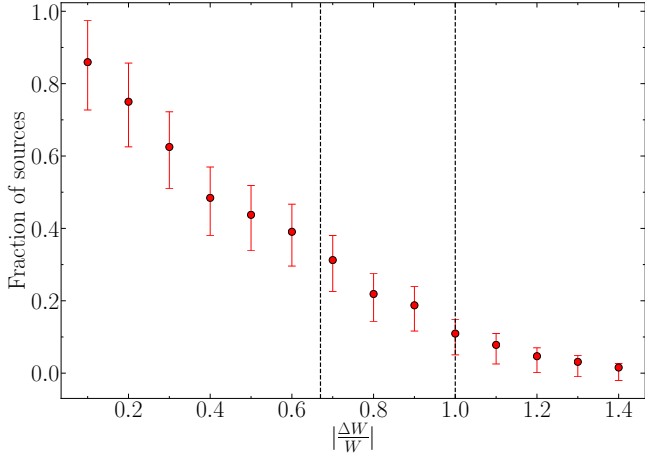


Figure 6. Fraction of sources showing C IV absorption variability larger than a certain threshold value of $|\frac{\Delta W}{W}|$ vs the threshold value $|\frac{\Delta W}{W}|$. Vertical dashed lines mark $|\frac{\Delta W}{W}|$ corresponding to equivalent width variations by a factor 2 and 3 respectively. Roughly 33% of quasars in our sample have UFO BALs showing W changing by a factor of 2 during our monitoring period.

cient number of measurements, C IV BALs tend to show significant equivalent width variability at all time scales.

Next, we consider the fraction of epoch pairs in a given time bin that is showing significant equivalent width variability. For our UFO BAL sample we find 0.78 ± 0.08 , 0.81 ± 0.05 , 0.85 ± 0.05 , 0.89 ± 0.07 for the time intervals 0.1–0.5, 0.5–2.0, 2.0–3.5, >3.5 yrs respectively. This once again confirms the highly variable nature of BAL troughs in our UFO BAL sample. When we repeat the same exercise for the full sample of Hemler et al. (2019) we find 0.27 ± 0.01 , 0.43 ± 0.01 , 0.47 ± 0.01 for 0–0.1, 0.1–0.5, 0.5–2.0 yrs bins respectively. The difference between the two samples is interesting. This could be either due to a difference in the properties of the quasars or to the more frequent sampling at smaller time scales in the case of Hemler et al. (2019). The typical sampling time scale between consecutive epochs in this study varies between less than a day to a few days where we expect the absorption line variation to be less.

In Fig. 6, we plot the fraction of sources showing C IV equivalent width variability between two epochs larger than a certain threshold $|\frac{\Delta W}{W}|$ as a function of $|\frac{\Delta W}{W}|$. This fraction decreases with increasing $|\frac{\Delta W}{W}|$ threshold. The percentage of sources showing $|\frac{\Delta W}{W}|$ greater than 0.67 and 1.0 (corresponding to equivalent width variations by a factor of 2 and 3 respectively) are 33% and 11% respectively as shown in Fig 6. In the sample of Hemler et al. (2019) 26% of the BAL quasars show $|\frac{\Delta W}{W}| > 0.67$. When we consider only BAL quasars satisfying our definition of UFOs the fraction increases to 40%. In the following discussions, we refer to BAL components with $|\frac{\Delta W}{W}| > 0.67$ as “highly variable” BALs. In the case of Lundgren et al. (2007) $\sim 9\%$ of the BALs are “highly variable” (at time-scales of ≤ 102 days) and this becomes $\sim 17\%$ if we consider the BALs that satisfy our condition to be an UFO BAL. In the sample of Gibson et al. (2008) $\sim 8\%$ of BALs are “highly variable” over a time scale of 3–6 yrs. Even in the sample of (Filiz Ak et al. 2013) we find only $\sim 8\%$ of the BAL studied are highly variable. Thus it appears that UFO BALs tend to show equivalent width

variations more frequently and with large amplitudes compared to the general BAL population.

Since most of the BALs in our sample show significant C IV equivalent width variations, it is interesting to study BALs that show roughly stable general profiles with insignificant equivalent width variations. It is possible that the non-detection of significant equivalent width variability in these types of sources can be attributed to the unavailability of a sufficient number of spectroscopic epochs. Alternatively, the absorption profile variation may be complex (i.e., uncorrelated over the full profile) and not perfectly captured by the equivalent width variations. This may be the case for some of the BALs which are spread over a few ten thousand km s^{-1} and consist of multiple narrow variable regions varying in an uncorrelated manner. To address such cases, we should consider pixel-based analysis which we plan to present in an upcoming paper. In our sample, the most dramatic BAL profile variation which resulted in the largest W change of 35 \AA is observed in J1156+0856 (3 epochs).

4.2 Time dependence of C IV BAL variability

Next, we study the variability of the C IV BAL equivalent width and its dependence on the time interval probed. In the top and middle panels of Fig. 7, respectively, we plot $\frac{\Delta W}{W}$ and ΔW as a function of the quasar rest frame time interval for all possible pairs of epochs (see Eqs. 1 and 2 for definitions). In the two panels the best-fit relationship obtained by Filiz Ak et al. (2013) is over-plotted as red solid curves. We can see that a significant number of our data points lie beyond these curves. In the bottom panel of Fig. 7, we show $\frac{\Delta W}{W}$ as a function of the maximum C IV rest equivalent width between the two epochs considered. The two horizontal dashed lines in the top and bottom panels indicate a fractional variability of ± 0.67 (i.e., “highly variable” BALs). We note that the scatter in both $\frac{\Delta W}{W}$ and ΔW is larger at longer time scales. It is also evident that the C IV equivalent width variations by more than a factor of 2 (or $|\frac{\Delta W}{W}| \geq 0.67$) occur only on large time-scales (i.e., > 0.2 yr) in our sample.

From the bottom panel of Fig. 7, it is evident that there is very little scatter in $\frac{\Delta W}{W}$ when the maximum C IV rest equivalent width is more than 55 \AA . On the other hand, a large scatter in $\frac{\Delta W}{W}$ is seen at small C IV equivalent widths (i.e. $< 5 \text{ \AA}$). We do find a nearly uniform scatter in $\frac{\Delta W}{W}$ in the middle range of maximum C IV equivalent widths. Also, we note that the occurrence of epoch pairs with $|\frac{\Delta W}{W}| > 0.67$ (i.e., “highly variable” BAL) is independent of C IV rest equivalent width in this middle W range.

Overall, we have 42 (52), 32 (40), 64 (80), and 36 (46) individual sources (or BALs) contributing 131, 287, 291, and 192 pairs of epochs respectively in 0.1–0.5, 0.5–2.0, 2.0–3.5, and 3.5–7.5 yrs time bins. In these 4 time bins the fraction of UFO BAL quasars having at least one BAL component that is “highly variable” are 0.12, 0.16, 0.23 and 0.28. The same for the BAL components are 0.14, 0.18, 0.20 and 0.24 respectively. Thus there is a clear indication in our sample that the fraction of “highly variable” BALs increases with increasing time intervals. For the first three time-bins the fraction of “highly variable” BALs are 0.01, 0.08 and 0.11 for the BALs studied in Filiz Ak et al. (2013). This once again confirms our finding that UFO BALs are more variable com-

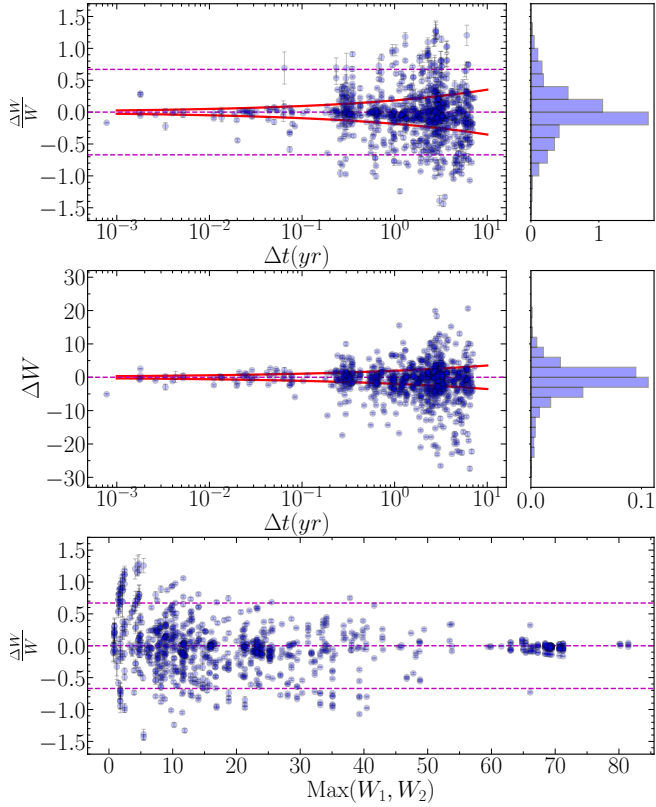


Figure 7. *Top panel* : This figure shows the $\frac{\Delta W}{W}$ distribution for the full sample as explained in Section 4.2 along with the histogram (right panel). Horizontal dotted lines mark $\frac{\Delta W}{W} = 0, \pm 0.67$ (i.e a factor 2 variation in W_{CIV}). *Middle panel* : This figure shows the ΔW distribution for the full sample with histogram (right panel). In both panels the red curves are the best fit relationship obtained by Filiz Ak et al. (2013). *Bottom panel* : This figure shows the $\frac{\Delta W}{W}$ vs ΔW distribution for the full sample where horizontal dotted lines mark $\frac{\Delta W}{W} = 0, \pm 0.67$. Note that the apparent “track” of points located close to each other mostly arises when the $\text{max}(W_1, W_2)$ remains the same but $\frac{\Delta W}{W}$ keeps changing between various epochs for a single object.

pare to the general BAL population. In the time bin 2.0–3.5 yrs (where all quasars in our sample contribute) the number of UFO BAL quasars showing $\frac{\Delta W}{W} > +0.67$ (6 BALs) and $\frac{\Delta W}{W} < -0.67$ (7 BALs) are nearly identical. Three BALs show both positive and negative variations with $|\frac{\Delta W}{W}| > 0.67$ in this time bin. However, in the 3.5–7.5 yrs time bin, we find a low fraction of UFO BAL quasars and BAL components showing $\frac{\Delta W}{W} > 0.67$ (3 BAL components) compared to that showing $\frac{\Delta W}{W} < -0.67$ (7 BAL components). Interestingly, for the 2.0–3.5 yrs time-bin, the number of “highly variable” BALs showing a negative trend is roughly a factor two higher than those showing positive trend in the sample of Filiz Ak et al. (2013). This may indicate that the growth and decay of C IV equivalent width may have different characteristic time scales. We will investigate this in more detail below.

We quantify the time dependence of C IV equivalent width variability using the inter-quantile range (IQR) as an indicator of the strength of variability for different time scales. We consider the same four time bins discussed above

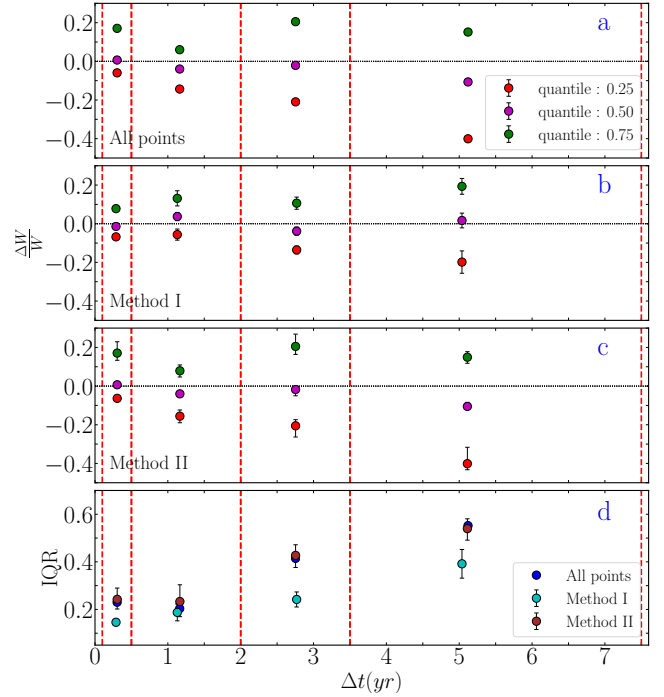


Figure 8. In the top three panels, we show the mean and sigma of quantiles at 0.25, 0.5 and 0.75 of $\frac{\Delta W}{W}$ distribution using all the points in the $\frac{\Delta W}{W}$ distribution (panel a), using method I (panel b) and method II (panel c) as described in Section 4.2, for four different time bins. In panel d, we show the IQR of $\frac{\Delta W}{W}$ distribution as calculated by different methods using quantiles shown in the top 3 panels. In each panel, the vertical red dashed lines mark the four Δt bins used for the analysis.

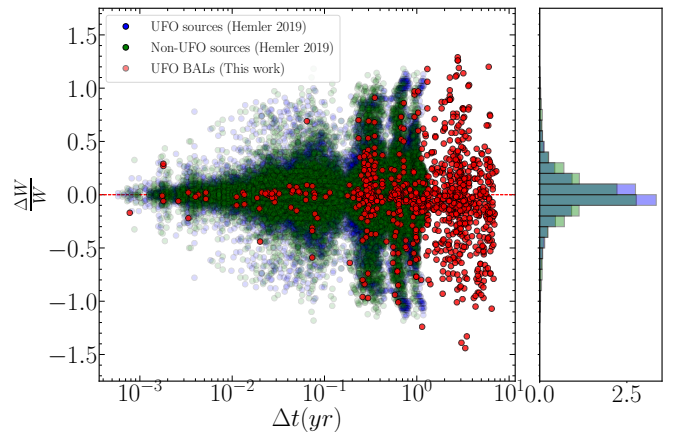


Figure 9. This figure shows the $\frac{\Delta W}{W}$ as a function of time for UFO (blue) and non-UFO (green) sources. For comparison, points from our UFO sample (red) is also shown.

and compute the quantiles at 0.25, 0.50, and 0.75 of the $\frac{\Delta W}{W}$ distribution for each time bin considering all points in the $\frac{\Delta W}{W}$ distribution shown in Fig. 7. The quantiles and the IQR estimated from these are shown in panels (a) and (d) of Fig. 8, respectively, for the four time bins. We observe an increasing trend in IQR with increasing time intervals with values of $0.23^{+0.04}_{-0.04}$, $0.20^{+0.07}_{-0.06}$, $0.41^{+0.04}_{-0.05}$, and $0.55^{+0.04}_{-0.05}$ for the four time bins in the ascending order. This indicates

that the scatter in $\frac{\Delta W}{W}$ increases with time (as found in past studies e.g. Capellupo et al. 2011; Filiz Ak et al. 2013).

As shown in the top panel of Fig. 3, the number of spectroscopic epochs varies strongly from one source to the other in our sample (see Table 1). In order to probe any bias in the $\frac{\Delta W}{W}$ distribution due to this non-uniform time sampling, we use two alternate methods to estimate the IQR. In the first method (hereafter method I), for each time bin, we randomly choose one measurement of $\frac{\Delta W}{W}$ per BAL and measure the quantiles at 0.25, 0.50, and 0.75 and IQR for the derived $\frac{\Delta W}{W}$ distribution. We repeat this procedure 1000 times and calculate the mean and σ of the resulting IQR distribution. Results using this method are shown in panel (b) of Fig. 8. The final IQR values are 0.18 ± 0.03 , 0.22 ± 0.04 , 0.26 ± 0.03 , and 0.39 ± 0.07 for 0.1-0.5, 0.5-2.0, 2.0-3.5, and 3.5-7.5 yrs time bins respectively.

In the second method (hereafter method II), we randomly choose 50 out of 64 sources and re-sample 64 sources from this sub-sample with replacement. We then calculate IQR for each time bin using all points from the randomly selected sources. We repeat this procedure 100 times and the mean and σ of the resulting IQR distribution are estimated. The final values of quantiles at 0.25, 0.50, and 0.75 and the IQR estimates are shown in panels (c) and (d) of Fig. 8. The final IQR values are 0.24 ± 0.04 , 0.23 ± 0.07 , 0.42 ± 0.05 and 0.53 ± 0.06 for 0.1-0.5, 0.5-2.0, 2.0-3.5 and 3.5-7.5 yrs time bins respectively. These values are even closer (i.e well within 1σ) to the ones obtained using the full sample. This exercise confirms that the increase in $\frac{\Delta W}{W}$ with time is not biased by non-uniform time sampling in our sample.

In addition, we looked at the width of the $\frac{\Delta W}{W}$ distribution after removing BALs having either very small or large W . For this, we considered only BALs with $5 < W_{max} < 55$ Å which corresponds to 69 out of the 80 BALs in our sample and carried out the same analysis to derive IQR values. Using method I, we obtained IQR values of 0.25 ± 0.03 , 0.36 ± 0.08 , 0.37 ± 0.04 , 0.61 ± 0.07 for 0.1-0.5, 0.5-2.0, 2.0-3.5, and 3.5-7.5 yrs time bins respectively. This confirms that the increase in the C IV equivalent width variability over time is not dominated by C IV BALs with large or small rest equivalent widths. In a similar way, we calculated the IQR for all the sources in the sample of Hemler et al. (2019) which turned out to be 0.11, 0.20, and 0.25 for 0-0.1, 0.1-0.5, and 0.5-2.0 years time bins respectively. This again suggests an increase with time of the scatter in the $\frac{\Delta W}{W}$ distribution as shown in Fig 9. There are two time bins that are common to our sample for which the IQR measured are consistent within a 1.5σ range.

4.3 Is the $\frac{\Delta W}{W}$ variation symmetric?

From Fig 8, we can see that the absolute value of the $\frac{\Delta W}{W}$ distribution quantiles at 0.25 and 0.75 are not the same in the 3.5-7.5 yrs time bin. This might suggest a possible asymmetry in our sample. This is what we study in this section. A symmetric distribution will indicate a statistically similar characteristic time-scale for increase/decrease in the C IV BAL absorption. Interestingly, while studying emerging/disappearing BAL components, several authors have noted (see for example, McGraw et al. 2017; Mishra et al. 2019) that the average time scales probed are higher for BAL disappearance events compared to the emergence

events. Discussions presented above also indicate that highly variable UFO BAL components tend to show a more negative trend in the 3.5–7.5 yrs time bin.

First, we carefully looked at the C IV rest equivalent width as a function of time for all objects in our sample to identify the presence of any monotonous trends either in the positive (i.e., increasing) or in the negative (decreasing) direction. Based on visual inspection, we classified the 80 BAL troughs in our sample into four classes: the ones showing (i) both considerable negative and positive ΔW variations, (ii) broadly positive ΔW variations (in these sources, there may be a few epochs with negative EW variations which are not significant compared to the general trend of variations), (iii) broadly negative ΔW variations and (iv) no systematic trend. The number of BALs in each category is 38, 16, 18, and 8 respectively. Thus, our sample does have 34 objects that show predominantly increasing or decreasing trends in the rest equivalent width as a function of time.

First, we consider the 3.5–7.5 yrs time bin, for which the quantiles plotted in the top 3 panels of Fig. 8 suggest a possible asymmetry towards the negative direction (i.e decreasing W). We measure the absolute difference in the values at 0.25 and 0.75 quantiles to be 0.25 ± 0.09 , 0.17 ± 0.07 and 0.25 ± 0.09 respectively for the values obtained using the full sample, method I and method II respectively. This suggests an asymmetry towards negative (decreasing W) at 2.4σ to 2.8σ level. We note however that 28% of the UFO BALs contributing to this time bin are “highly variable” BALs with the tendency to show negative variations. We thus probe the symmetry of the distribution after removing the 10 UFO BAL quasars in this bin that show “highly variable” BAL components. We find the distribution to be more symmetric with an absolute difference in the values at 0.25 and 0.75 quantiles to be 0.02 ± 0.04 when we use “method I”. The KS-test returns a p-value of 0.71. Thus the large asymmetry seen in this time bin is largely driven by “highly variable” BAL sources.

Next, we consider the 2.0–3.5 yrs time bin where all the 64 UFO BAL quasars in our sample contribute. We measure the absolute difference in the values at 0.25 and 0.75 quantiles to be 0.05 ± 0.06 , 0.01 ± 0.06 and 0.00 ± 0.06 respectively for the values obtained using the full sample, method I and method II respectively. This indicates a symmetric distribution in the positive and negative directions. The KS-test results confirm the same with a p-value of 0.36. Next, we ask whether the distribution remains symmetric when we avoid the 10 UFO BAL QSOs that show “highly variable” BALs in the 3.5–7.5 yrs time-bin. In this case we get the absolute difference in the values at 0.25 and 0.75 quantiles to be 0.07 ± 0.08 when we use “method I” and the KS-test p-values of 0.41. The distribution is found to be symmetric in any case.

Since the asymmetry seems to arise from highly variable BALs on longer timescales, we focus on the time evolution of 21 BAL components from the 20 quasars in our sample that show high variability ($|\frac{\Delta W}{W}| > 0.67$) for $\Delta t > 2$ yr. To begin with, for each highly variable BAL in this sub-sample, we plot the rest equivalent width, W , normalized by the maximum W (i.e., W_{max}) observed for that BAL against the time difference from the epoch where it attained the maximum W value (see Fig 10). Hence, the positive (negative) values in the abscissa correspond to epochs after (before) the maxi-

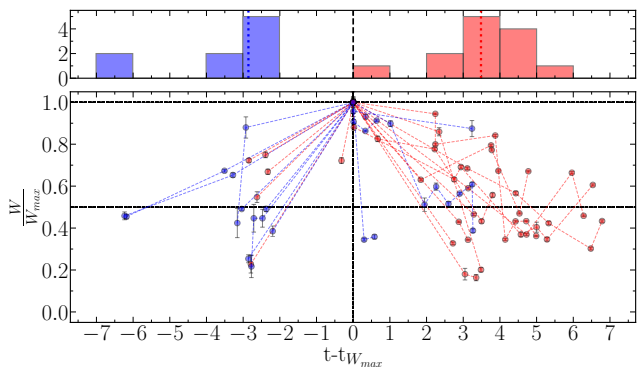


Figure 10. The C IV rest equivalent width (W) normalized by the maximum observed W (i.e., $\frac{W}{W_{max}}$) is plotted against the time difference (in year) from the epoch where it attained the maximum W value (i.e., $t-t_{W_{max}}$) for each BAL in the “highly variable” sub-sample. The blue points correspond to BALs which had the maximum change in $\frac{W}{W_{max}}$ in the increasing direction whereas the red correspond to the same in the decreasing direction. In the top panel, we plot the histogram of shortest $t-t_{W_{max}}$ at which $\frac{W}{W_{max}}$ crossed the 0.5 line with the median shown in dotted lines.

mum W is achieved. Here, we clearly see that there are more BALs that show large variability on the decreasing side compared to the increasing side. This has been discussed in detail in Section 4.2. Interestingly, we also observe that many BALs on the decreasing side (i.e., positive $t-t_{W_{max}}$) reach values less than $\frac{W_{max}}{2}$ (as indicated by the red dashed lines in Fig 10) at larger time scales of more than 4 yr. But, on the increasing side (i.e., negative $t-t_{W_{max}}$), among the comparatively lower number of BALs showing high variability, most of them increase to W_{max} from values less than $\frac{W_{max}}{2}$ at rather smaller time scales of ~ 3 yr. We notice that the time scales for the equivalent width to decrease by a factor of 2 are on average higher than that of increasing equivalent width cases (look at the histogram in the top panel of Fig. 10). As asymmetry seen in $\frac{\Delta W}{W}$ for this time bin is dominated by the “highly variable” BAL components this could be driven by the fact that the decreasing/disappearing time scale is generally longer than the increasing/appearing time scale. But it is good to keep in mind that when we study the appearing and disappearing BAL time scales, there can be a certain bias in the results due to the fact that all our BALs are fairly strong in the first epoch itself. This may affect the study of appearing time scales since we have missed the epochs when the BAL was formed.

4.4 Comparison with Filiz Ak et al. (2013) results

Filiz Ak et al. (2013) have obtained a relationship between the relative W variation $|\frac{\Delta W}{W}|$ and the minimum sampled rest-frame timescale Δt_{min} from the 428 BAL troughs identified in their sample (see equation 7 in their paper). As we noted in Fig. 7, our sample seems to show more scatter compared to this relationship. However, in order to perform a significant comparison we need to account for the differences in the distribution of minimum sampling time intervals (Δt_{min}) between their sample and our UFO sample (see Fig. 3). For this, we first calculate $\frac{\Delta W}{W}$ for all possible combinations of epochs for each source in the UFO sam-

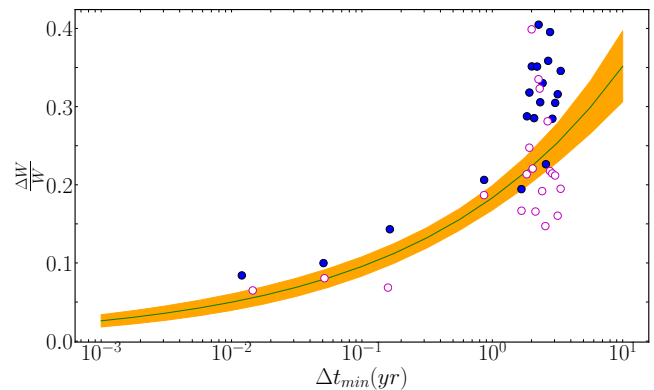


Figure 11. The fractional variation in W of C IV UFO BAL observed in our sample (circles, see Section 4.4) is plotted versus the minimum sampled rest-frame timescale Δt_{min} . The best-fit relation obtained in Filiz Ak et al. (2013) is overplotted as a blue curve and the shaded region shows its uncertainty. The empty circles represent the same comparison after removing the “highly variable” sources (as explained in Section 4.3) from the sample.

ple and populate the $|\frac{\Delta W}{W}|$ vs. Δt plane. Next, we resample 80 points from this plane with the time sampling consistent with a normalized Δt_{min} distribution as given in Filiz Ak et al. (2013) for the 428 distinct BAL troughs in their sample. Following Filiz Ak et al. (2013), we also do an average over 4 time-ordered data points from the above sampled points. This results in a total of 21 points. We repeat the above steps 1000 times and take the mean of each point from the total number of iterations. Now we compare these points (filled blue circles) with the best-fit relation from Filiz Ak et al. (2013) in Fig. 11. We observe that most of the points are located at a few years time-scale and almost all of them show much higher $|\frac{\Delta W}{W}|$ values than what is expected from the fit. This confirms that the UFO BALs in our sample are highly variable compared to the fit from Filiz Ak et al. (2013). This difference can not be attributed to the differences in the sampling of Δt . If we remove the 20 quasars with “highly variable” BALs and repeat the procedure, we derive measurements shown as open circles in Fig. 11 which are more consistent with the Filiz Ak et al. (2013) relation. This confirms that the behavior of $|\frac{\Delta W}{W}|$ is significantly influenced by the “highly variable” BALs.

4.5 What drives the BAL variability ?

In this section, we correlate $\frac{\Delta W}{W}$ with different BAL and quasar properties to investigate the physical conditions in UFO BALs and the possible origin of the equivalent width variations.

4.5.1 Dependence on the BAL properties

We consider four properties of the observed BAL troughs: the C IV equivalent width W , the optical depth weighted velocity centroid (v_{cent}), the maximum relative depth d_{BAL} and the velocity width ($\Delta V = v_{max} - v_{min}$) of the BAL trough. For each of these parameters, we divide the BAL sample into two sub-samples of equal number including the BALs with parameter values larger and smaller than their

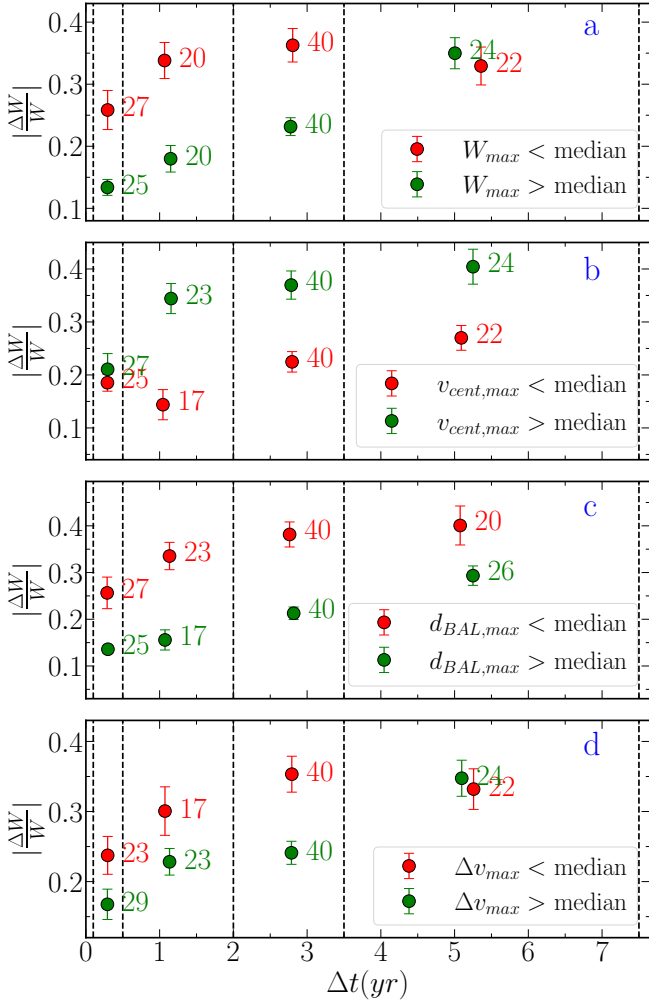


Figure 12. The average $|\frac{\Delta W}{W}|$ distribution of different sub-samples (W_{max} in panel a, optical depth weighted velocity centroid in panel b, maximum depth in panel c, and velocity width in panel d) defined below and above the median (see section 4.5.1) of different BAL properties for different time bins. Errors correspond to the standard deviation. The number of UFO BALs used for each measurement is also indicated in the figure.

median value. The median values are 21.2 \AA , 16434 km s^{-1} , 0.71 and 13939 km s^{-1} for maxima of W , v_{cent} , d_{BAL} and Δv of the BAL respectively.

For each source in these sub-samples, whenever available (as it is not necessary that all objects contribute to all the time bins considered) we randomly select a pair of epochs (and corresponding $|\frac{\Delta W}{W}|$) that falls in the four time bins considered here. We then measure the average $|\frac{\Delta W}{W}|$ for all sources in a sub-sample for each time bin. We repeat the above process 100 times and obtain the mean and standard deviation of the average $|\frac{\Delta W}{W}|$ distribution of the sub-samples for each time bin. Results are presented in Fig 12.

In the first three time bins (i.e., $\Delta t \leq 3.5$ yrs) we note that the average $|\frac{\Delta W}{W}|$ is higher for the sub-sample with lower equivalent width (i.e., $W_{max} < 21.2 \text{ \AA}$). The difference is larger than the 3.5σ level. This is not the case for larger time scales (>3.5 yrs). This is consistent with what we find in the bottom panel of Fig. 7, where a large scatter in $\frac{\Delta W}{W}$

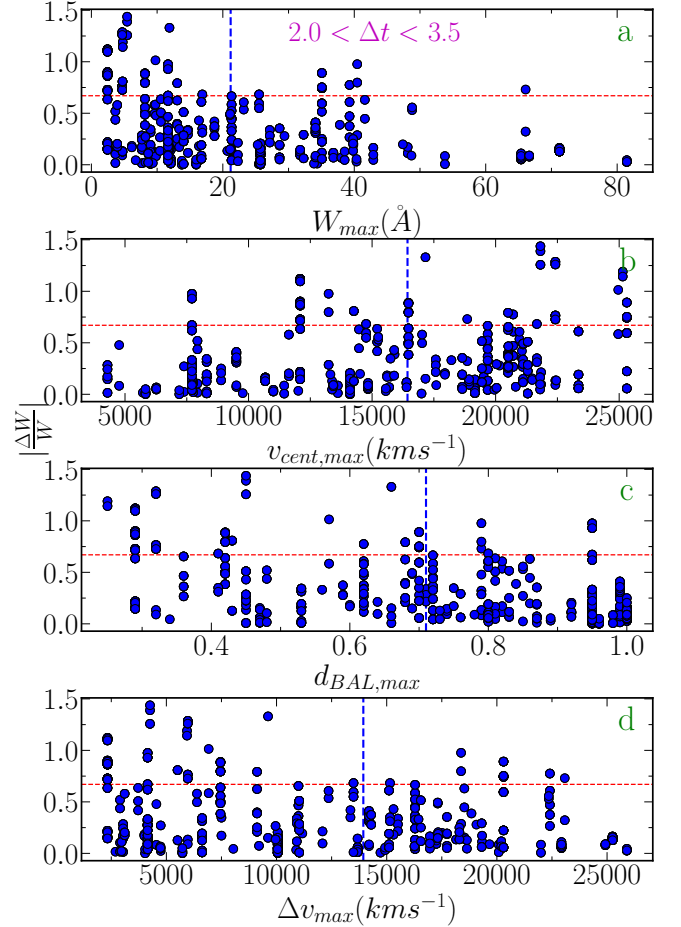


Figure 13. All the measured $|\frac{\Delta W}{W}|$ for each BAL component as a function of their properties for the time bin, $2.0 \leq \Delta t \leq 3.5$ yrs. The vertical dashed line in each panel indicates the median abscissa value. The horizontal line corresponds to $|\frac{\Delta W}{W}|=0.67$.

is seen for $W_{max} < 5$. In panel (a) of Fig. 13, we plot $|\frac{\Delta W}{W}|$ as a function of W_{max} for all the observed pairs in the time bin $2.0 \leq \Delta t \leq 3.5$ years (where all the 64 UFO BALs contribute). It is evident that the scatter in $|\frac{\Delta W}{W}|$ is larger when W_{max} is below the median value indicated by the vertical dashed line. A similar trend is seen for d_{BAL} (see panel (c) in Fig. 12 and Fig. 13). It is interesting to note that the trend is the same for the velocity widths (Δv). Note that, in Fig. 13, the points look discretized due to the relatively small changes in these parameter values plotted in the x-axis for a given object for all the epoch pairs considered. This means that absorption lines with low W having narrow and shallow absorption profiles tend to show large variability.

Some of the above findings are consistent with those of Filiz Ak et al. (2013) (refer to subsection 4.5 therein). They find that shallower BALs show more variability and report a highly significant correlation ($>99\%$), between ΔW , $\frac{\Delta W}{W}$ and average W in their sample (see also, Capellupo et al. 2011; Vivek et al. 2014; Hemler et al. 2019). However, contrary to our results, they find that wider BALs vary more than narrower ones and state that this is expected since wider BAL troughs might have a better chance of containing variable regions. This difference could be related to the way our UFO BALs sample is constructed which avoids BALs

that only have strong narrow absorption at low velocities (i.e., $v_{max} < 15000 \text{ km s}^{-1}$). We address this point in detail below. Also, recall [Filiz Ak et al. \(2013\)](#) have used one measurement per quasar obtained at the lowest time scale probed. Here, we use multiple epoch measurements for each quasar but sampled once for each time bin.

In low-resolution spectra, like the one we consider here, the equivalent width variations can be driven by (i) optical depth variations, (ii) variations in the covering factor (f_c ; see for example, [Muzahid et al. 2016](#)) and/or (iii) changes in the line of sight density and velocity field due to transverse velocity component (see for example, [Aromal et al. 2022](#)). At this stage, there is no obvious way to disentangle these possibilities which are all reasonably possible as it is easier to change the property of weak components compared to strongly saturated ones.

In panel (b) of Fig 12 we notice that the sub-sample with large v_{cent} shows a larger variability (significant at $>3 \sigma$ level) compared to the sub-sample with smaller v_{cent} for all time-scales $\Delta t > 0.5$ yrs. In the lowest time bin, $0.1 \leq \Delta t(\text{yrs}) \leq 0.5$, the difference between the two sub-samples is not statistically significant. In panel (b) of Fig. 13, we plot $|\frac{\Delta W}{W}|$ as a function of maximum v_{cent} for all the observed pairs in the time bin $2.0 \leq \Delta t(\text{yrs}) \leq 3.5$ years. It is evident from this plot that the scatter in $|\frac{\Delta W}{W}|$ is larger for a higher value of maximum v_{cent} . Similarly highly variable UFO BALs are more frequent when v_{cent} is larger. This is consistent with the finding of [Filiz Ak et al. \(2013\)](#) that the high-velocity BALs vary more than lower-velocity ones. They interpret this as a secondary effect based on the fact that higher-velocity absorption has lower W . However, in our sample, we do not find any significant anti-correlation between W_{max} and v_{cent} (with a Spearman's correlation coefficient of -0.02 and p-value of 0.85). Thus it is not obvious that the dependence of v_{cent} is a secondary effect. To further investigate this, we note that ten out of 80 BAL components have $v_{cent} < 8000 \text{ km s}^{-1}$ and tend to have low equivalent widths (i.e., $< 20 \text{ \AA}$). If we do not consider these 10 low-velocity components having low W_{max} we do find indeed a moderate anti-correlation between W_{max} and v_{cent} (with a Spearman correlation coefficient of -0.32 and p-value of 0.01). We come back to this in a bit more detail below.

Note that in the case of simple disk wind models (as well as when gas motions are assumed to be nearly Keplerian), large velocities are related to gas components ejected closer to the accretion disk ([Arav et al. 1994](#)). In this kind of scenario v_{cent} could well be the primary parameter of large $|\frac{\Delta W}{W}|$. Further [Proga et al. \(2012\)](#) demonstrated that C IV absorption produced by disk wind models from hydrodynamical simulations is quite complex and the simulated C IV absorption profiles show large variability, especially at high velocities. They attribute this excess variability at large velocities to the emergence of very fast mass ejections from relatively large distances, where the gas is well shielded from X-ray radiation. As we do not have independent distance measurements for different velocity components we will not be able to test such a scenario using our data. To summarize the results presented here demonstrate that, in general, more fractional equivalent width variability is observed in weak, high-velocity, and shallow BALs.

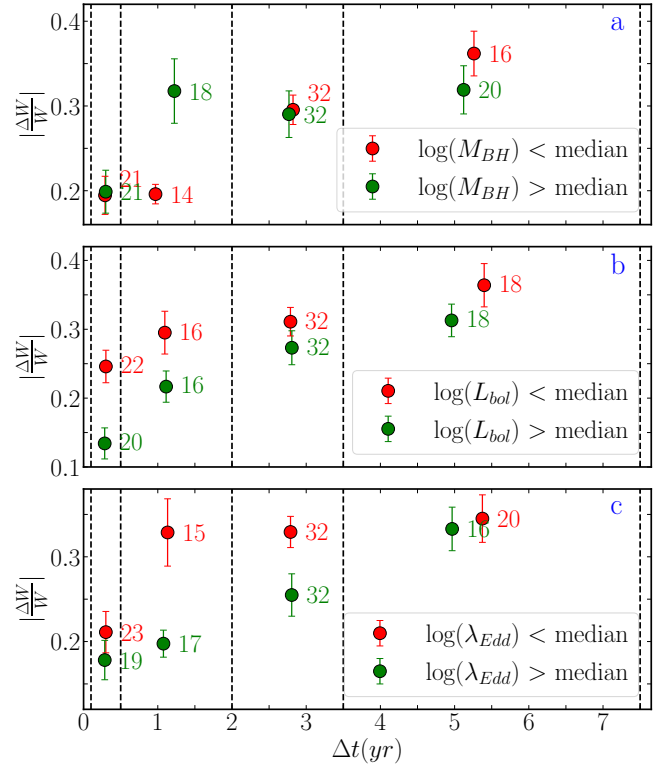


Figure 14. Same as Fig. 12 for M_{BH} (panel a), L_{bol} (panel b), and λ_{Edd} (panel c).

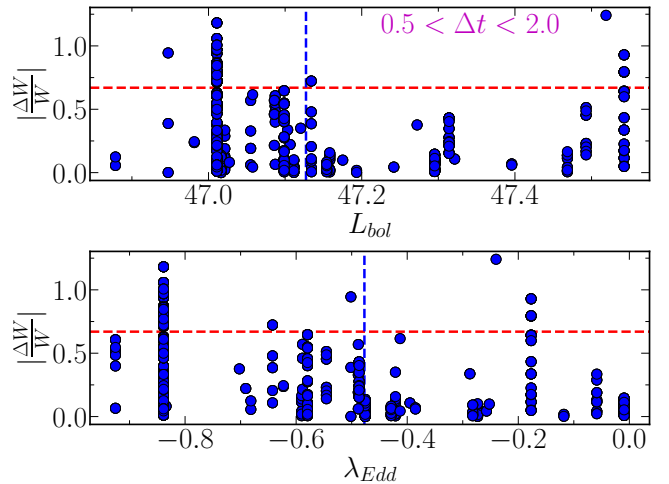


Figure 15. $\frac{\Delta W}{W}$ is shown for each UFO BAL as a function of L_{bol} (top panel) and λ_{Edd} (bottom panel) for the time bin $0.5 < \Delta t < 2.0$ yrs. The vertical dashed line indicates the median value of the quantity in the abscissa and the horizontal line indicates $|\frac{\Delta W}{W}| = 0.68$.

4.5.2 Dependence on the quasar properties

In this section, we explore whether the variations in $|\frac{\Delta W}{W}|$ are related to any of the following quasar properties: M_{BH} , λ_{Edd} and bolometric luminosity L_{bol} . For this, we again compare the $|\frac{\Delta W}{W}|$ distributions of two sub-samples defined as the objects having one of the above parameters smaller vs. larger than the median value of the whole UFO sample. Fol-

lowing the same procedure as described above, we obtain the mean and standard deviation of $|\frac{\Delta W}{W}|$ in four time bins for each sub-sample. Results are summarized in Fig. 14.

In the largest time bin (i.e., $3.5 \leq t(\text{yrs}) \leq 7.5$) the variations of $|\frac{\Delta W}{W}|$ are clearly independent of the quasar properties considered here. When we combine this with the discussions presented in the previous sub-section, it appears that for the largest time-scales only v_{cent} seems to be related to the relative W variations indicating that this may be an important parameter for the interpretation of these flows at large time scales (i.e., $t > 3.5 \text{ yrs}$).

In the case of L_{bol} and λ_{Edd} , $|\frac{\Delta W}{W}|$ is found to be higher for low L_{bol} and low λ_{Edd} compare to high L_{bol} and high λ_{Edd} in all the three short time bins (i.e., for $\Delta t < 3.5 \text{ yrs}$ in Fig. 14). In particular for $0.5 \leq \Delta t < 2.0 \text{ yrs}$, $|\frac{\Delta W}{W}|$ shows a large difference between sub-samples defined based on all three properties considered here (see Fig. 14). As mentioned before, this time bin gets contributions from only 32 quasars with 40 UFO BALs in our sample. To explore this further, we plot $|\frac{\Delta W}{W}|$ vs. L_{bol} (top panel) and λ_{Edd} (bottom panel) in Fig. 15 for the time bin $0.5 \leq \Delta t(\text{yrs}) \leq 2.0$. We do see the scatter to be larger towards lower L_{bol} and λ_{Edd} . However, we find (unlike in the case of v_{cent} or W_{max}) no clear tendency for the ‘‘highly variable’’ BAL components to have any preference for low L_{bol} or λ_{Edd} . Also due to the limiting magnitude used for defining our sample quasar properties of the objects in our sample may not span the full range spanned by the general population of quasars (see Fig. 2). Therefore, it would be good to confirm the differences seen in $|\frac{\Delta W}{W}|$ for different sub-sample using more measurements.

For the sake of comparison, we use an approach similar to that of Filiz Ak et al. (2013) and consider $|\frac{\Delta W}{W}|$ for the shortest time scale for each source. Except for L_{bol} which shows a moderate anti-correlation (Spearman’s coefficient = -0.31 , p-value=0.01), both M_{BH} and λ_{Edd} show no evidence of correlation. Similarly, when we consider the $|\frac{\Delta W}{W}|$ over the longest time scale for each source we do not find any correlation with any of these quasar parameters. Filiz Ak et al. (2013) found a large scatter in the ΔW distribution for sources with low L_{bol} on moderate (1-2.5 yr) and long ($>2.5 \text{ yr}$) time scales compared to high L_{bol} sources. However, they could not find any significant correlation using rank-correlation analysis except for moderate time scales (1-2.5 yrs). They also did not find evidence for a correlation between λ_{Edd} and scatter in either ΔW or $\frac{\Delta W}{W}$.

In the case of M_{BH} significant (i.e., at 3.6σ level) difference is seen between our two sub-samples only in the $0.5 \leq \Delta t(\text{yrs}) \leq 2.0$ time bin. Filiz Ak et al. (2013) did not find any evidence for the presence of correlation between M_{BH} and $\frac{\Delta W}{W}$ in their sample. On the other hand, He et al. (2015) found that there is a medium strong negative correlation ($r=-0.537$, $p=0.003$) between ΔW and Mg II based M_{BH} estimates in 28 BAL QSOs with variable BAL regions.

In summary, in our sample, there is no strong evidence of any correlation between the BAL variations and the characteristics of the quasars.

4.5.3 Do highly variable UFO BAL quasars have different properties?

As mentioned before, 24 BAL components in 21 UFO BAL quasars in our sample tend to be ‘‘highly variable’’. In this

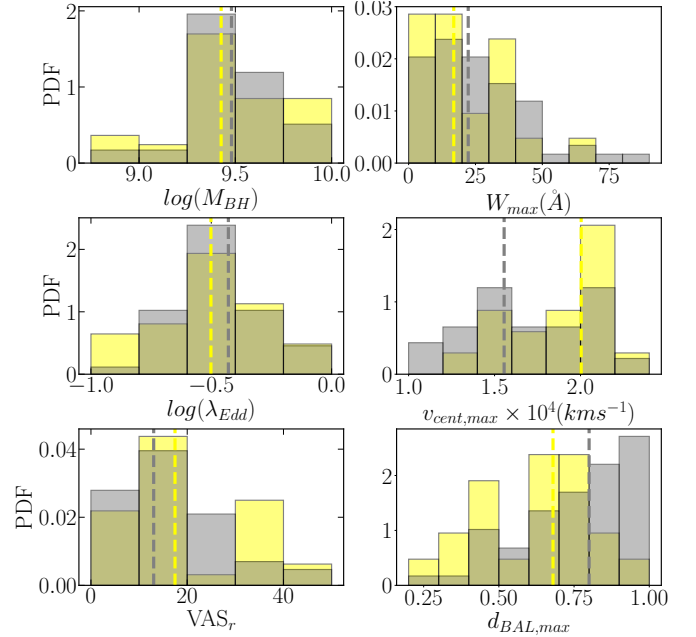


Figure 16. Distribution of quasar (left panels) and BAL (right panels) properties of ‘‘highly variable’’ UFO BALs (shown in yellow) and the rest of the UFO sample (gray). Vertical dashed lines indicate the median values for each histogram.

section, we compare the properties of these ‘‘highly variable’’ UFO BALs with those of the rest of the UFO BALs in our sample. In Fig. 16 we compare the distributions of quasar properties (M_{BH} , λ_{Edd} and VAS_r as introduced in Section 3.1) and BAL properties (W_{max} , maximum of v_{cent} and maximum of d_{BAL}) for ‘‘highly variable’’ BALs and the rest of our sample. The median value of each distribution is shown as a vertical (gray or yellow) dashed line in each panel.

For quasar properties, we find that the M_{BH} and λ_{Edd} distributions are similar for both sub-samples (p-value is >0.1 from the KS test) whereas for VAS_r the p-value is 0.03 for the KS test. This indicates that occurrence of ‘‘highly variable’’ BAL is not strongly coupled to M_{BH} or λ_{Edd} . However, there is an indication that the UFO BAL quasars showing ‘‘highly variable’’ BALs tend to show slightly larger photometric variability compared to the rest of the UFO quasars. This could either mean the large equivalent width variabilities are driven by photoionization or disk instabilities that also results in photometric variability. We come back to this discussion in more detail in section 4.8.

For BAL properties, the distributions of W_{max} are identical as indicated by p-value > 0.1 from the K-S test (see also Fig. 16). However a larger fraction of ‘‘highly variable’’ BALs have comparatively higher values of $v_{cent,max}$ and lower values of $d_{BAL,max}$. K-S test p-values are 0.01 and 0.03 for $v_{cent,max}$ and $d_{BAL,max}$ respectively. In summary, we find that ‘‘highly variable’’ BALs tend to have comparatively shallower absorption at higher velocities. A considerable fraction of UFO BALs with ‘‘highly variable’’ components tend to show excess variability in their r-band light curves.

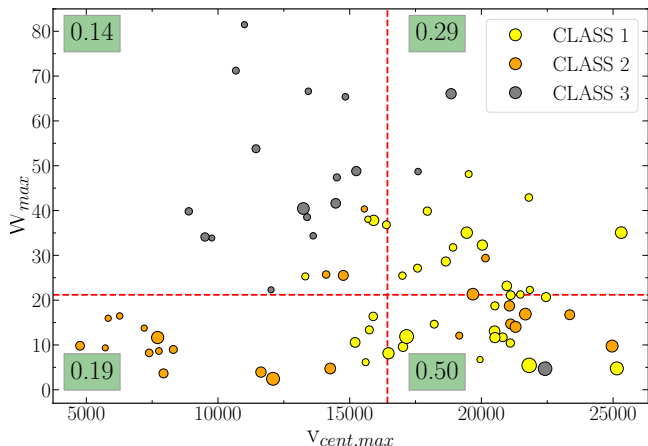


Figure 17. Maximum W (W_{max}) as a function of maximum v_{cent} ($v_{cent,max}$) for all the UFO BALs in our sample. The class of each UFO BAL is indicated by the color as shown in the legend and the size of the circle scales with the maximum $|\frac{\Delta W}{W}|$ observed. The red dashed lines show the median along the respective axis and the fraction of sources with $\max(|\frac{\Delta W}{W}|) > 0.67$ is indicated in green boxes for the corresponding regions of the plane.

4.6 Different classes of UFOs

Here we investigate whether there is a relation between the scatter in $|\frac{\Delta W}{W}|$ and the overall BAL profile. For this, we classify quasars in our UFO sample into three classes based on the global absorption profile structure. Typical examples are shown in Fig. 1. **Class-1:** Includes sources with one or more C IV UFO BALs having $v_{min} > 8000 \text{ km s}^{-1}$ without any C IV broad absorption at lower velocities (top panel in Fig. 1). There are 33 sources in our sample that were classified as Class-1. In three of these cases (J0224-0528, J1054+0150 and J1317+0100) there are two UFO BAL-components with $v_{min} > 8000 \text{ km s}^{-1}$. In the remaining 30 sources there is only one C IV BAL complex. Basically, BALs in this class are well detached from the C IV emission line without any low-velocity absorption. **Class-2:** Includes only sources with multiple BAL troughs having at least one UFO BAL with $v_{min} > 8000 \text{ km s}^{-1}$ and one non-UFO BAL with $v_{min} < 8000 \text{ km s}^{-1}$. In this case, the UFO BAL and non-UFO BAL components are distinguishable (middle panel of Fig. 1). There are 13 objects in our sample that belongs to this class. In three cases (J0046+0104, J0242+0049 and J2352+0105) the low-velocity BAL complex has $v_{max} < 3000 \text{ km s}^{-1}$ and is not listed in Table 1. In two sources (J2310+0746 and J1322+0524) we have identified three distinct BAL complexes with one of them being a UFO BAL and the other two being present at lower velocities. **Class-3:** Contains sources with a single UFO BAL trough having $v_{min} < 8000 \text{ km s}^{-1}$ (bottom panel of Fig. 1). This class, by definition, has absorption spread over a wide range of velocities and absorption from distinct components are merged into a single BAL component when we follow the definition of Filiz Ak et al. (2013). There are 17 sources in our sample that are classified as Class-3. Only one UFO BAL quasar, J0216+0115, could not be classified as the absorption profile does not fit with any of the definitions of the three classes mentioned above. Column 8 in Table 1 provides the classification for each quasar in our sample.

Note, the classification scheme discussed here is motivated by the two-component (polar and equatorial) wind models discussed in Borguet & Hutsemékers (2010). In this model, absorption profiles consistent with that of Class-3 will have contributions from both fast-moving polar and slow-moving equatorial winds seen at low inclination angles. Detached profiles as those of Class-1 will mainly come from fast-moving polar components seen at high inclination angles to the disk plane. Thus the classification we adopt may reflect a classification based on the inclination angle with respect to the disk. While this gives a motivation for the above classification scheme, we are aware that a given absorption profile can be produced by models with a wide range of parameters.

The fraction of “highly variable” sources are 0.30 (10/33), 0.54 (7/13), and 0.18 (3/17) for Class-1, Class-2 respectively. This indicates the possible connection between profile shapes and variability of C IV absorption. To explore this further, we study how UFO BAL quasars belonging to different classes populate the W_{max} vs. v_{cent} plane (see Fig. 17). The low-velocity absorption components of Class-2 populate mostly the bottom left part of the plane whereas the high-velocity components populate the bottom right part. Class-3 populates mostly the upper left part of the plane as expected because the BAL extends continuously to large velocities with v_{cent} being typically in the lower side. Class-1 objects populate both the upper and lower quarters of the upper half of v_{cent} . The size of each point in Fig. 17 is proportional to the amplitude of $|\frac{\Delta W}{W}|$. The fraction of UFO BALs showing “highly variable” BALs are indicated in each quadrant in Fig. 17. Nearly 50% of the BALs in the high v_{cent} and low W_{max} show $|\frac{\Delta W}{W}| > 0.67$. This quadrant is mainly populated by Class-1 and high-velocity component of Class-2 BALs in our sample. This implies that the relatively weaker and detached high-velocity BALs have a tendency to show more variability. On the other hand, a lower fraction (i.e., 14%) of UFO BALs seems to be “highly variable” in the low v_{cent} and high W_{max} quadrant. This quadrant is predominantly occupied by Class-3 BALs. In the quadrant with low W_{max} and low v_{cent} we find only 19% of the BALs are “highly variable”. This quadrant is predominantly occupied by low-velocity components of Class-2 BALs in our sample. On the other hand, in the quadrant with high v_{cent} and high W_{max} nearly 29% of BALs are “highly variable”. *All this clearly imply that high C IV BAL variability is associated with both large v_{cent} and W_{max} and W_{max} alone is not a primary driver of the large variability.*

Next, we study the $\frac{\Delta W}{W}$ distribution of UFO BALs in different classes as a function of time (see Fig. 18). The histograms in the right panels of Fig. 18 show the distributions of $\frac{\Delta W}{W}$ in each case. It is apparent that the scatter in the distribution is decreasing from Class-1 to Class-2 followed by Class-3. This result may be affected by the different number of sources in each class. To confirm the trend seen in Fig. 18, we measure IQR for different classes using method-I (see Section 4.2) for the four time bins (i.e., 0.1-0.5, 0.5-2.0, 2.0-3.5, and 3.5-7.5 yrs). IQR values obtained for Class-1 are 0.27 ± 0.03 , 0.45 ± 0.10 , 0.40 ± 0.05 , and 0.60 ± 0.08 respectively. For Class-2, IQR values for the UFO BALs (i.e. only for the high-velocity components) are 0.29 ± 0.12 , 0.46 ± 0.15 , 0.49 ± 0.11 , and 0.43 ± 0.13 respectively. The IQR values for

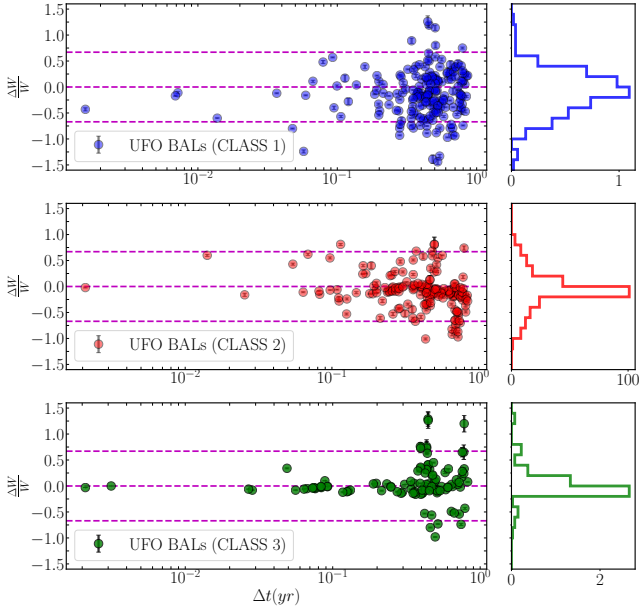


Figure 18. This figure shows the $\frac{\Delta W}{W}$ vs time for UFOs in Class 1 (top panel), Class 2 (middle panel), and Class 3 (bottom panel) sources. The panels in the right side show the histogram distribution of $\frac{\Delta W}{W}$. Horizontal dashed lines mark $\frac{\Delta W}{W} = 0$ and ± 0.67 . It is evident that Class-1 and Class-2 UFO BALs show larger scatter compared to that of Class-3.

Class-1 and Class-2 objects are consistent within errors. However, for Class-3, IQR values are 0.06 ± 0.01 , 0.07 ± 0.02 , 0.22 ± 0.06 , and 0.61 ± 0.01 respectively. Clearly, Class-3 objects show consistently lower IQR values (compared to the other two classes) except for the longest-time bin of 3.5-7.5 years.

Next, we probe the possible correlation between the $\frac{\Delta W}{W}$ distributions of the distinct low- and high-velocity BAL troughs seen in Class-2 sources (i.e., UFO and non-UFO BALs). From the top panel of Fig 19, it is clear that the variations in high- and low-velocity BAL troughs are correlated. Also, using the linear regression, we find a slope of 0.95 considering all the class 2 sources whereas if we exclude BAL components towards J1322+0524 that contribute an appreciable number of points to this plot, the slope turns out to be 1.45. This indicates that the UFO BALs show more variability compared to non-UFO BALs in general, but in the case of J1322+0524, the UFO and non-UFO BALs vary with similar strength leading to a slope close to 1. Also, from the bottom panel of Fig 19, we see that the $\frac{\Delta W}{W}$ distributions of high- and low-velocity BALs are considerably different (p-value = 0.04) with high-velocity BALs showing more scatter than the low-velocity ones. This is consistent with what was shown before: high-velocity BALs are more variable.

To extend this analysis to Class-3 objects, we divide the continuous absorption profile into two regions above and below the velocity mid point, $v_{mid} = \frac{v_{min} + v_{max}}{2}$. Even in this case (see Fig. 20), we find a correlated variability between high- and low-velocity regions as in the case of Class-2 sources, but with a much steeper slope (1.95) indicating that high-velocity regions are much more variable compared

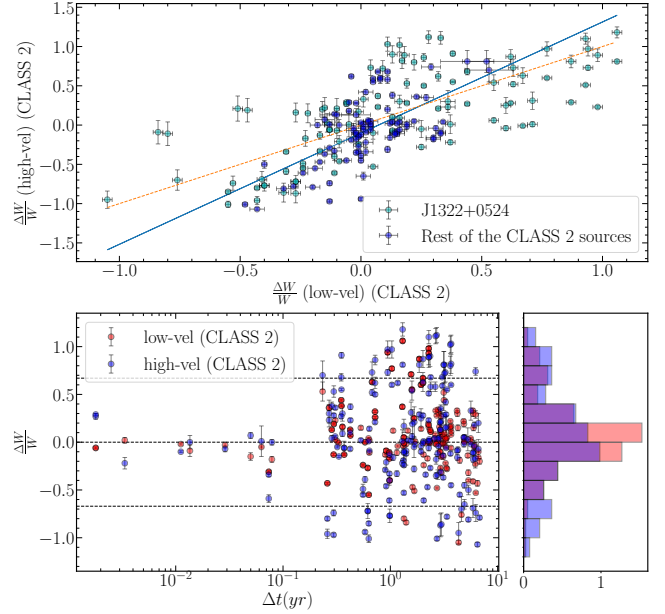


Figure 19. *Top panel:* Comparison of $\frac{\Delta W}{W}$ of low-velocity non-UFO BAL troughs to that of UFO BALs in Class-2 sources. The points contributed by J1322+0524 (cyan) are shown separately. The blue line is the best-fitted linear regression line. The equality line is shown by the orange dotted line. *Bottom panel:* The $\frac{\Delta W}{W}$ distribution of non-UFO (red) and UFO BALs (blue) in Class-2 sources as a function of time. Horizontal dashed lines mark $\frac{\Delta W}{W} = 0$ and ± 0.67 .

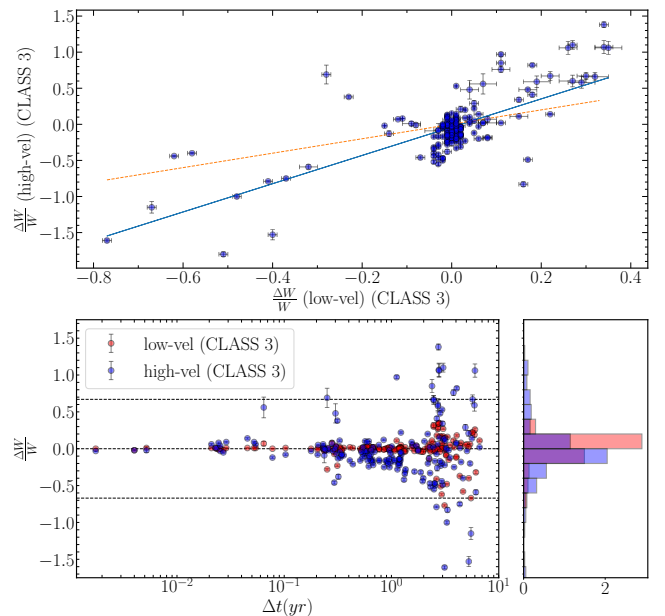


Figure 20. *Top panel:* $\frac{\Delta W}{W}$ of low-velocity vs. $\frac{\Delta W}{W}$ of high-velocity regions in quasars belonging to Class-3. The blue line shows the best-fitted linear regression line. The equality line is indicated by the orange dotted line. *Bottom panel:* $\frac{\Delta W}{W}$ of low- and high-velocity regions of BAL troughs belonging to Class-3 as a function of time. Horizontal dashed lines mark $\frac{\Delta W}{W} = 0$ and ± 0.67 .

to low-velocity ones. We should remember that this is due in part to the fact that low-velocity regions are more saturated.

4.7 C IV emission lines and BAL connection

As discussed in Section 3.2, we measured the equivalent width (W_{BEL}) and the blueshift (BS_{BEL}) of the C IV emission line in a sub-sample of 41 UFO BALs with v_{min} larger than 6000 km s^{-1} so that the C IV emission profile is not affected by the absorption. By definition, all 33 objects in Class-1 are part of this sample. In the remaining 8 sources, 2 and 6 sources belong to Class-2 and -3 respectively. As seen in Section 3.2 and Fig. 5, BS_{BEL} is much larger for UFO BAL quasars compared to non-BAL quasars. The measured large values of BS_{BEL} in BAL quasars are assumed to be a consequence of outflowing gas in the BLR.

We searched for correlations by calculating Spearman’s correlation coefficient and corresponding p-values (see Table 2) between BS_{BEL} or $\max(\Delta W_{BEL}/W_{BEL})$ with the BAL parameters W_{max} , $v_{cent,max}$, v_{max} , $d_{BAL,max}$ and Δv_{max} . From Table 2, we observe a strong correlation between BS_{BEL} and W_{max} , v_{max} and $d_{BAL,max}$ whereas a moderate correlation is reported for Δv_{max} . These strong correlations are consistent with recent studies including Rankine et al. (2020) who found that BAL quasars with the highest W_{BEL} and lowest BS_{BEL} tend to show weaker, narrower, and comparatively low-velocity BAL troughs and vice-versa. Rodríguez Hidalgo & Rankine (2022) also reported that the maximum velocity of EHVO increases with blueshift as seen in our sample. This seems to suggest that the high velocity BAL phenomenon is intimately related to the blueshift of the C IV emission line.

For each pair of epochs, we measured the fractional equivalent width changes in C IV BAL and BEL. The Spearman rank correlation test (with a coefficient of -0.05 and p-value of 0.47) confirms the lack of any correlation between the two quantities. Note that for a couple of individual cases with enough observations, we do find a possible correlation between the two quantities (see Aromal et al. 2021, 2022). The lack of a similar correlation for the full sample is probably related to the insufficient time sampling that fails to detect the delayed response from the BEL regions. Establishing such a correlation is important to confirm the ionization-induced BAL variations.

Next, we divide our sample into two around the median BS_{BEL} . Then compared the mean value of $|\frac{\Delta W}{W}|$ in the four time-bins considered in this study. We find a significant difference only for the third time-bin, i.e., 2.0-3.5 yrs. For this time bin, we looked at the $|\frac{\Delta W}{W}|$ distribution as a function of BS_{BEL} as shown in Fig 21. It is clear from the figure that the sources with less blueshift tend to show larger scatter in the $|\frac{\Delta W}{W}|$ distribution. The Spearman rank correlation test suggests a possible anti-correlation with a coefficient of -0.25 and a p-value of <0.001 . This may be explained as the result of a moderate correlation of W_{max} with blueshift from Table 2 combined with the fact that BALs with low W show more variability. It is difficult to confirm these trends given the limited size of the sample, but future studies with larger sample sizes and better time sampling can help in reaching stronger conclusions.

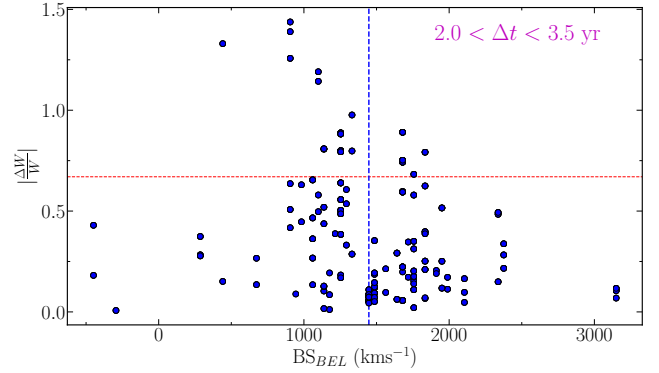


Figure 21. $\frac{\Delta W}{W}$ is shown for each UFO BAL source as a function of blueshift for the time bin $2.0 < \Delta t < 3.5$ yrs. The vertical dashed line indicates the median value of the quantity in the abscissa and the horizontal line indicates $|\frac{\Delta W}{W}| = 0.68$.

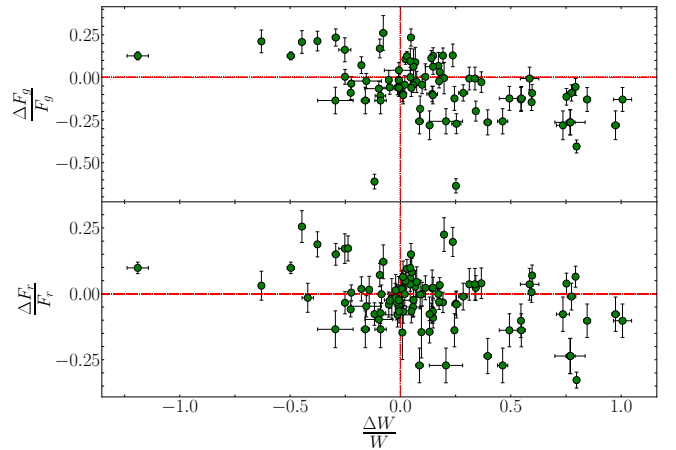


Figure 22. In this figure, we compare the fractional variations in total g- and r- band flux to that of the BAL EW in the top and bottom panels respectively.

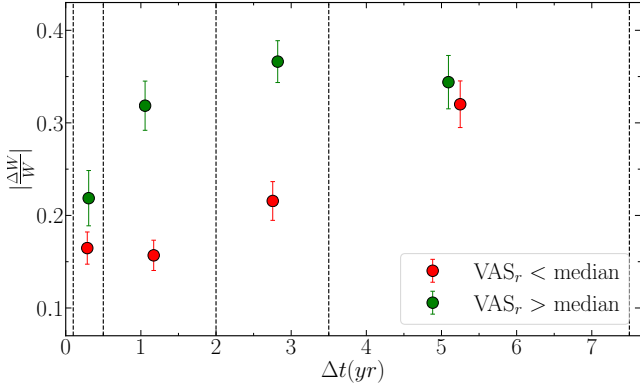
4.8 Are continuum variations related to BAL variability ?

As mentioned before, we have obtained publicly available light curves to see the trends in continuum variations during our spectroscopic monitoring period. From Section 3.1, it is clear that the variability amplitude strength (VAS) follows the same distribution irrespective of the presence of BALs. This implies that the continuum variations of our UFO BAL quasars are not very different from the general quasar population. However, we also notice that the distribution of VAS in the r-band is different for “highly variable” UFO BALs and the rest of the UFO BALs in our sample (see Fig. 16).

Here, we explore the possible connection between the continuum variability and the variability of C IV equivalent width in our UFO BAL sample. We consider photometric epochs in g- and r-bands which are within 10 days in the observer’s frame (roughly 3 days in the rest-frame) to our spectroscopic epochs whenever available and convert them to flux units. Using these, we compare the fractional variations in total g- and r- band flux (F_g and F_r respectively) to that of the rest equivalent width of the C IV BAL. As shown in Fig 22, we see moderate anti-correlation with high significance between $\frac{\Delta F_g}{F_g}$ and $\frac{\Delta W}{W}$ with spearmann coefficient, $r =$

Table 2. Dependence of BAL properties on properties of C IV broad emission line

Sample	Spearman coefficient, p value				
	W_{max}	$v_{cent,max}$	v_{max}	$d_{BAL,max}$	Δv_{max}
BS_{BEL}	0.340, 0.021	0.093, 0.538	0.351, 0.016	0.336, 0.022	0.272, 0.068
$\max(\frac{\Delta W_{BEL}}{W_{BEL}})$	-0.447, 0.005	0.041, 0.805	-0.151, 0.364	-0.392, 0.015	-0.417, 0.009

**Figure 23.** We plot the mean and standard deviation of the average $\frac{\Delta W}{W}$ distribution at the four different time-scales, i.e. short (0-0.5 yr), intermediate (0.5-2 yr) and two long (2-3.5 yr and >3.5 yr) time-scales, for the two sub-samples having estimated VAS of the r-band light curve below and above its median.

-0.48 , p-value = 3.50×10^{-6} and weak anti-correlation with lesser significance between $\frac{\Delta F_r}{F_r}$ and $\frac{\Delta W}{W}$ with $r = -0.25$, p-value = 1.34×10^{-2} . In order to demonstrate that this effect is not dominated by the sources having a large number of epochs, we remove sources having more than 8 epochs of spectroscopic observations and carry out the same analysis to find even stronger anti-correlation signatures with $r = -0.62$, p-value = 1.27×10^{-5} for g-band and $r = -0.34$, p-value = 1.92×10^{-2} for r-band. While the anti-correlation is statistically significant, we do see the spread in the fractional variation in the continuum flux is smaller than that of C IV rest equivalent width.

The analysis indicates that the continuum flux variations may be responsible for the observed BAL variability where the W of the C IV BAL decreases as the continuum increases. This is in agreement with several other studies. Lu et al. (2018) found the same trend with similar r-coefficient, $r = -0.43$ with p-value $< 1e-44$ between the fractional variations of the absorption C IV equivalent width and that of the monochromatic continuum luminosity at 1450 Å calculated from the spectra. Mishra et al. (2019) showed that the dimming in the continuum is associated with the appearance of new BALs. Horiuchi et al. (2020) also looked at a few of the SDSS RM sources and found a possible presence of correlation between the BAL variability and photometric variability using iPTF and PanSTARRS surveys.

To ascertain this tendency, we also divided the sources into two sub-samples based on the VAS values in r-band (r-band is preferred over g-band since most BALs coincide with g-band region whereas r-band is little affected by the same) and looked at the average of $|\frac{\Delta W}{W}|$ in different time bins similarly to the analysis performed in Section 4.5.3. The results are shown in Fig. 23. It is clear that except for the 4th time bin, sources with large photometric variability also

show consistently higher BAL variability up to 3.5 years in rest-frame time scales.

Aromal et al. (2022) while analyzing the multiple epoch spectroscopic observations of three BAL components in J1322+0524 found that the amplitude of optical continuum flux variations is much smaller than what is needed to produce the observed equivalent width variations. Based on this and a large scatter in W found for a given continuum flux they argued that C IV ionizing continuum and optical continuum need not vary in a correlated manner and the amplitude of ionizing continuum variation has to be much higher than what we see in the optical light curves. From Fig. 22, we see scatter in the equivalent width fractional variations are much larger than that seen in the continuum. This implies the conclusions drawn in the case of J1322+0524 may still be valid for most of the UFO BALs in our sample. Therefore, it will be interesting to probe the rest frame FUV variability of our UFO BAL quasars.

5 RESULTS AND DISCUSSIONS

In this work we have presented an analysis of the C IV absorption variability of 80 distinct BAL components observed in the spectra of 64 UFO BAL quasars. We used spectra from SDSS together with our own data from SALT. Our monitoring time-scale spans between a few months to ~ 7 yrs in the quasar rest frame. Here, we mainly focus on the variability of the C IV rest equivalent width. We will present details of pixel-based optical depth analysis and a detailed study of interesting sources (as in Aromal et al. 2021, 2022) in future papers. The main results from this study are :

1) BAL variability fraction: We find the C IV absorption in $\sim 95\%$ of UFO BALs vary (by $\geq 3\sigma$) at least once during our monitoring. Roughly 33% of quasars in our sample show “highly variable” (i.e., $|\frac{\Delta W}{W}| > 0.67$) BAL components. Also, independent of the source and time scale considered, $\sim 80\%$ of epoch pairs show significant variations. These percentages are higher than what is reported for the general BAL population in the literature. For example, when we consider only the pair of observations separated by the shortest time-scale for each object, $\sim 70\%$ of UFO BAL QSOs and UFO BAL components show significant variability which is a higher occurrence than that found by Filiz Ak et al. (2013). The shortest time intervals probed here being shorter than that of Filiz Ak et al. (2013) one may have expected less variability in our sample. All this indicates that UFO BALs are more variable compared to the normal BAL population.

2) Time dependence of BAL variability: We study the variability of the C IV rest equivalent width in four different time-bins (i.e., 0.1-0.5, 0.5-2.0, 2.0-3.5 and 3.5-7.5 yrs) in the quasar rest frame. The inter quartile range (IQR) of $\frac{\Delta W}{W}$ increases with increasing time scale which means that the

variations become larger with increasing time scale. This result is not influenced by the different time-sampling achieved for different sources and is not related to any particular behavior of systems with low ($W < 5\text{\AA}$) or high ($W > 55\text{\AA}$) C IV rest equivalent widths. We also note that the fraction of “highly variable” BALs increases with increasing time scale. Such “highly variable” C IV BALs dominate the large variability seen at long time scales. By comparing our data (with appropriate time sampling) with the $\frac{\Delta W}{W}$ -vs. t relationship of Filiz Ak et al. (2013) we show our UFO BALs are more variable compared to the overall BAL population.

A larger fraction of UFO BALs in our sample show a negative $\frac{\Delta W}{W}$ in the largest time-bin (3.5-7.5 yrs). In addition, using the time evolution of C IV rest equivalent width in 21 BAL components that show large variability over a time-scale > 2 yrs, we find that a decrease in rest equivalent width by a factor of two occurs over a longer time-scale (i.e., a median of ~ 3.5 yrs) compared to an increase by the same amount (i.e., a median of ~ 2.8 yrs). This is consistent with the finding that the average time scales are higher for BAL disappearance events compared to the emergence events (see, McGraw et al. 2017; Mishra et al. 2019). Confirming our results for the full sample through our ongoing monitoring programme will provide a possible link between the large equivalent width variability and extreme events like emergence/disappearance of BALs.

3) Dependence of BAL variability on quasar properties : We find no significant dependence of BAL variability on quasar properties like M_{BH} , L_{bol} and λ_{Edd} even though a moderate correlation is observed for L_{bol} on time scales less than 2 yrs. This is consistent with what has been found in the overall population of C IV BALs (see for example, Filiz Ak et al. 2013). We do notice that the properties of QSOs in our sample do not probe the same range as what we see in the general population of quasars. This may have limited our ability to detect any weak trend. While some quasars in our sample show large C IV BEL variations insufficient time-sampling related to the expected reverberation time-scales prevents us from correlating the C IV BEL and UFO BAL variabilities. In cases where such detailed investigation is possible we do see large BEL variations in quasars that show large UFO BAL variations (see Aromal et al. 2021, 2022). Spectroscopic monitoring, at shorter time intervals, of a sub-sample of quasars in our sample that show significant C IV BEL variations would be very useful.

We find that on an average the optical photometric variability of quasars in our sample are not statistically distinguishable from that of our control sample. However, we do find an anti-correlation between the optical continuum flux variations (in both g- and r-band) and variations in C IV BAL equivalent width. In addition, the scatter in $|\frac{\Delta W}{W}|$ is more for objects showing VAS value larger than the median of our sample compared to the rest of the objects. All these are consistent with the absorption variability being somehow linked to the continuum flux variations. However, the spread in the fractional flux variations is much smaller than that of W . In a simple photo-ionization scenario this would imply much larger amplitude for the variability of the C IV ionizing flux compared to that in the rest frame NUV range probed by the optical variability. It will be interesting to

check the relationship between the variability NUV flux and C IV ionizing flux using direct measurements

4) Dependence of BAL variability on BAL properties : By studying the variability nature of different sub-samples based on the C IV absorption properties, we find that weak, high-velocity, shallow, and low-width BALs tend to show more variability than others. Similarly the “highly variable” BAL components tend to be shallow having large velocities and narrow widths. We find that detached C IV BAL components with large ejection velocities show larger equivalent width variations. In general C IV equivalent width variations are by and large correlated across the velocity profile. However, the amplitude of $\frac{\Delta W}{W}$ is larger in the case of high velocity components compared to their low-velocity counterparts. Based on this we suggest that both low-equivalent width and high-velocity are equally important to determine the strength of variability in a BAL.

5) Reconciling with physical models? : Proga et al. (2000); Proga & Kallman (2004) use axisymmetric, time-dependent hydrodynamical simulations of radiation-driven disk winds in AGN to conclude that radiative line driving is efficient enough to accelerate disk winds to high velocities as seen in BALs. However the variable C IV absorption produced by such simulated disk winds depends on a complex velocity field and covering factor (Proga et al. 2012). We note that the simulated C IV absorption profiles in their study show high variability, especially at high velocities. They attribute this excess of variability at large velocities to the emergence of very fast mass ejections from relatively large distances, where the gas is well shielded from X-ray radiation.

The best way to constrain such models is to compare the gas density, covering factor and distance of the absorbing cloud from the continuum source in the model with the constraints coming from observation. For this we need high resolution spectroscopic observations of our objects covering a larger rest wavelength range (Srianand & Petitjean 2000). Alternatively, it will be interesting to ask whether observed properties like (i) the $\frac{\Delta W}{W}$ vs. t relationship, (ii) the time-scale of decreasing equivalent width being higher than that of increasing equivalent width, (iii) the lack of strong correlations with quasar properties, (iv) the connection between BEL blueshift and C IV absorption line variability, (v) the observation of large equivalent variability when there is no large optical continuum variations and (vi) the importance of low equivalent width and high velocity to produce high amplitude variation etc., can be reproduced by hydrodynamical simulations. Additional constraints for models can be obtained from pixelated optical depth analysis. We will be presenting results of such an analysis for our sample in our upcoming paper.

ACKNOWLEDGEMENTS

We thank Aseem Paranjape and K. Subramanian for useful discussions. PA thanks Labanya K Guha for helpful discussions on several python programming techniques used in this paper. PPJ thanks Camille Noûs (Laboratoire Cogitamus) for inappreciable and often unnoticed discussions, advice and support. PPJ is partly supported by the Agence Nationale de la Recherche under contract ???.

Funding for SDSS-III has been provided by the Alfred P. Sloan Foundation, the Participating Institutions, the National Science Foundation, and the U.S. Department of Energy Office of Science. The SDSS-III web site is <http://www.sdss3.org/>.

SDSS-III is managed by the Astrophysical Research Consortium for the Participating Institutions of the SDSS-III Collaboration including the University of Arizona, the Brazilian Participation Group, Brookhaven National Laboratory, Carnegie Mellon University, University of Florida, the French Participation Group, the German Participation Group, Harvard University, the Instituto de Astrofísica de Canarias, the Michigan State/Notre Dame/JINA Participation Group, Johns Hopkins University, Lawrence Berkeley National Laboratory, Max Planck Institute for Astrophysics, Max Planck Institute for Extraterrestrial Physics, New Mexico State University, New York University, Ohio State University, Pennsylvania State University, University of Portsmouth, Princeton University, the Spanish Participation Group, University of Tokyo, University of Utah, Vanderbilt University, University of Virginia, University of Washington, and Yale University.

DATA AVAILABILITY

Data used in this work are obtained using SALT. Raw data will become available for public use 1.5 years after the observing date at <https://ssda.sao.ac.za/>.

REFERENCES

- Allen J. T., Hewett P. C., Maddox N., Richards G. T., Belokurov V., 2011, *MNRAS*, **410**, 860
- Arav N., 1996, *ApJ*, **465**, 617
- Arav N., Li Z.-Y., Begelman M. C., 1994, *ApJ*, **432**, 62
- Arav N., Liu G., Xu X., Stidham J., Benn C., Chamberlain C., 2018, *ApJ*, **857**, 60
- Aromal P., Srianand R., Petitjean P., 2021, *MNRAS*, **504**, 5975
- Aromal P., Srianand R., Petitjean P., 2022, *MNRAS*, **514**, 1975
- Barlow T. A., Junkkarinen V. T., Burbidge E. M., Weymann R. J., Morris S. L., Korista K. T., 1992, *ApJ*, **397**, 81
- Baskin A., Laor A., Stern J., 2014, *MNRAS*, **445**, 3025
- Bellm E. C., et al., 2019a, *PASP*, **131**, 018002
- Bellm E. C., et al., 2019b, *PASP*, **131**, 068003
- Borguet B., Hutsemékers D., 2010, *A&A*, **515**, A22
- Borguet B. C. J., Arav N., Edmonds D., Chamberlain C., Benn C., 2013, *ApJ*, **762**, 49
- Bowler R. A. A., Hewett P. C., Allen J. T., Ferland G. J., 2014, *MNRAS*, **445**, 359
- Brotherton M. S., Tran H. D., Becker R. H., Gregg M. D., Laurent-Muehleisen S. A., White R. L., 2001, *ApJ*, **546**, 775
- Buckley D. A. H., Charles P. A., Nordsieck K. H., O'Donoghue D., 2005, *Proceedings of the International Astronomical Union*, **1**, 1–12
- Burgh E. B., Nordsieck K. H., Kobulnicky H. A., Williams T. B., O'Donoghue D., Smith M. P., Percival J. W., 2003, in Iye M., Moorwood A. F. M., eds, Society of Photo-Optical Instrumentation Engineers (SPIE) Conference Series Vol. 4841, Instrument Design and Performance for Optical/Infrared Ground-based Telescopes. pp 1463–1471, [doi:10.1117/12.460312](https://doi.org/10.1117/12.460312)
- Capellupo D. M., Hamann F., Shields J. C., Rodríguez Hidalgo P., Barlow T. A., 2011, *MNRAS*, **413**, 908
- Capellupo D. M., Hamann F., Shields J. C., Rodríguez Hidalgo P., Barlow T. A., 2012, *MNRAS*, **422**, 3249
- Capellupo D. M., Hamann F., Shields J. C., Halpern J. P., Barlow T. A., 2013, *MNRAS*, **429**, 1872
- Chambers K. C., et al., 2016, arXiv e-prints, [p. arXiv:1612.05560](https://arxiv.org/abs/1612.05560)
- Chen Z., He Z., Ho L. C., Gu Q., Wang T., Zhuang M., Liu G., Wang Z., 2022, *Nature Astronomy*, **6**, 339
- Crawford S. M., et al., 2010, in Silva D. R., Peck A. B., Soifer B. T., eds, Society of Photo-Optical Instrumentation Engineers (SPIE) Conference Series Vol. 7737, Observatory Operations: Strategies, Processes, and Systems III. p. 773725, [doi:10.1117/12.857000](https://doi.org/10.1117/12.857000)
- Dai X., Shankar F., Sivakoff G. R., 2008, *ApJ*, **672**, 108
- De Cicco D., Brandt W. N., Grier C. J., Paolillo M., Filiz Ak N., Schneider D. P., Trump J. R., 2018, *A&A*, **616**, A114
- Dunn J. P., et al., 2010, *ApJ*, **709**, 611
- Elvis M., 2000, *ApJ*, **545**, 63
- Filiz Ak N., et al., 2012, *ApJ*, **757**, 114
- Filiz Ak N., et al., 2013, *ApJ*, **777**, 168
- Foltz C. B., Weymann R. J., Morris S. L., Turnshek D. A., 1987, *ApJ*, **317**, 450
- Gehrels N., 1986, *ApJ*, **303**, 336
- Gibson R. R., Brandt W. N., Schneider D. P., Gallagher S. C., 2008, *ApJ*, **675**, 985
- Gibson R. R., et al., 2009, *ApJ*, **692**, 758
- Gibson R. R., Brandt W. N., Gallagher S. C., Hewett P. C., Schneider D. P., 2010, *ApJ*, **713**, 220
- Guo H., Shen Y., Wang S., 2018, PyQSOFit: Python code to fit the spectrum of quasars, Astrophysics Source Code Library ([ascl:1809.008](https://ui.adsabs.org/abs/ascl:1809.008))
- Hall P. B., et al., 2013, *MNRAS*, **434**, 222
- He Z.-C., Bian W.-H., Ge X., Jiang X.-L., 2015, *MNRAS*, **454**, 3962
- Hemler Z. S., et al., 2019, *ApJ*, **872**, 21
- Hewett P. C., Wild V., 2010, *MNRAS*, **405**, 2302
- Higginbottom N., Knigge C., Long K. S., Sim S. A., Matthews J. H., 2013, *MNRAS*, **436**, 1390
- Hopkins P. F., Elvis M., 2010, *MNRAS*, **401**, 7
- Horiuchi T., Morokuma T., Misawa T., Hanayama H., Kawaguchi T., 2020, *AJ*, **159**, 237
- Kobulnicky H. A., Nordsieck K. H., Burgh E. B., Smith M. P., Percival J. W., Williams T. B., O'Donoghue D., 2003, in Iye M., Moorwood A. F. M., eds, Society of Photo-Optical Instrumentation Engineers (SPIE) Conference Series Vol. 4841, Instrument Design and Performance for Optical/Infrared Ground-based Telescopes. pp 1634–1644, [doi:10.1117/12.460315](https://doi.org/10.1117/12.460315)
- Kormendy J., Ho L. C., 2013, *Annual Review of Astronomy and Astrophysics*, **51**, 511
- Law N. M., et al., 2009, *PASP*, **121**, 1395
- Lu W.-J., Lin Y.-R., Qin Y.-P., 2018, *MNRAS*, **473**, L106
- Lundgren B. F., Willhite B. C., Brunner R. J., Hall P. B., Schneider D. P., York D. G., Vanden Berk D. E., Brinkmann J., 2007, *ApJ*, **656**, 73
- Matthews J. H., Knigge C., Long K. S., Sim S. A., Higginbottom N., Mangham S. W., 2016, *MNRAS*, **458**, 293
- McGraw S. M., et al., 2017, *MNRAS*, **469**, 3163
- Mishra S., Gopal-Krishna Chand H., Chand K., Ojha V., 2019, *MNRAS*, **489**, L42
- Murray N., Chiang J., Grossman S. A., Voit G. M., 1995, *ApJ*, **451**, 498
- Muzahid S., Srianand R., Charlton J., Eracleous M., 2016, *MNRAS*, **457**, 2665
- Ostriker J. P., Choi E., Ciotti L., Novak G. S., Proga D., 2010, *ApJ*, **722**, 642
- Pâris I., et al., 2017, *A&A*, **597**, A79
- Proga D., Kallman T. R., 2004, *ApJ*, **616**, 688
- Proga D., Stone J. M., Kallman T. R., 2000, *ApJ*, **543**, 686

- Proga D., Rodríguez-Hidalgo P., Hamann F., 2012, in Chartas G., Hamann F., Leighly K. M., eds, *Astronomical Society of the Pacific Conference Series Vol. 460, AGN Winds in Charleston*. p. 171 ([arXiv:1201.3606](https://arxiv.org/abs/1201.3606)), [doi:10.48550/arXiv.1201.3606](https://doi.org/10.48550/arXiv.1201.3606)
- Rankine A. L., Hewett P. C., Banerji M., Richards G. T., 2020, *MNRAS*, **492**, 4553
- Reichard T. A., et al., 2003, *AJ*, **126**, 2594
- Richards G. T., et al., 2006, *ApJS*, **166**, 470
- Rodríguez Hidalgo P., Rankine A. L., 2022, *ApJ*, **939**, L24
- Rodríguez Hidalgo P., Khatri A. M., Hall P. B., Haas S., Quintero C., Khatu V., Kowash G., Murray N., 2020, *ApJ*, **896**, 151
- Rogerson J. A., Hall P. B., Ahmed N. S., Rodríguez Hidalgo P., Brandt W. N., Filiz Ak N., 2018, *ApJ*, **862**, 22
- Shen Y., et al., 2011, *ApJS*, **194**, 45
- Silverman B. W., 1986, *Density estimation for statistics and data analysis*
- Srianand R., Petitjean P., 2000, *A&A*, **357**, 414
- Srianand R., Petitjean P., Ledoux C., Hazard C., 2002, *MNRAS*, **336**, 753
- Stalin C. S., Srianand R., Petitjean P., 2011, *MNRAS*, **413**, 1013
- Temple M. J., Banerji M., Hewett P. C., Rankine A. L., Richards G. T., 2021, *MNRAS*, **501**, 3061
- Tombesi F., Cappi M., Reeves J. N., Palumbo G. G. C., Yaqoob T., Braito V., Dadina M., 2010, *A&A*, **521**, A57
- Tombesi F., Cappi M., Reeves J. N., Nemmen R. S., Braito V., Gaspari M., Reynolds C. S., 2013, *MNRAS*, **430**, 1102
- Vaughan S., Edelson R., Warwick R. S., Uttley P., 2003, *MNRAS*, **345**, 1271
- Vestergaard M., Peterson B. M., 2006, *ApJ*, **641**, 689
- Vivek M., Srianand R., Petitjean P., Mohan V., Mahabal A., Samui S., 2014, *MNRAS*, **440**, 799
- Vivek M., Srianand R., Dawson K. S., 2018, *MNRAS*, **481**, 5570
- Wampler E. J., Chugai N. N., Petitjean P., 1995, *ApJ*, **443**, 586
- Wang H., Xing F., Zhang K., Wang T., Zhou H., Zhang S., 2013, *ApJ*, **776**, L15
- Weymann R. J., Morris S. L., Foltz C. B., Hewett P. C., 1991, *ApJ*, **373**, 23
- Yi W., et al., 2020, *ApJ*, **893**, 95
- de Kool M., Begelman M. C., 1995, *ApJ*, **455**, 448

APPENDIX A: ESTIMATION OF QUASAR PROPERTIES

In this section, we explain how we estimate different quasar properties and compare the same to Shen et al. (2011). We obtain M_{BH} using the FWHM of the C IV emission measured from the spectrum using the empirical mass-scaling relationship given by Vestergaard & Peterson (2006) and the bolometric luminosity using bolometric correction to the monochromatic luminosity at 1350 Å derived from the composite SED from Richards et al. (2006). Note that for these measurements, we used the SDSS spectrum with the highest SNR available for each object.

Now, we compare our estimated values with that of Shen et al. (2011) for both M_{BH} and L_{bol} for 38 sources in our UFO sample and 20 non-BAL quasars from our control sample as shown in Fig A1. It is clear that Shen et al. (2011) tends to over-predict M_{BH} and under-predict L_{bol} for BAL quasars compared to their non-BAL counterparts as shown by the shift in respective distributions. We find that this may be due to the continuum fits used in Shen et al. (2011) which uses conventional line-free regions for the fitting that may still include BAL regions, leading to incorrect estimation of quasar properties. This mostly lead

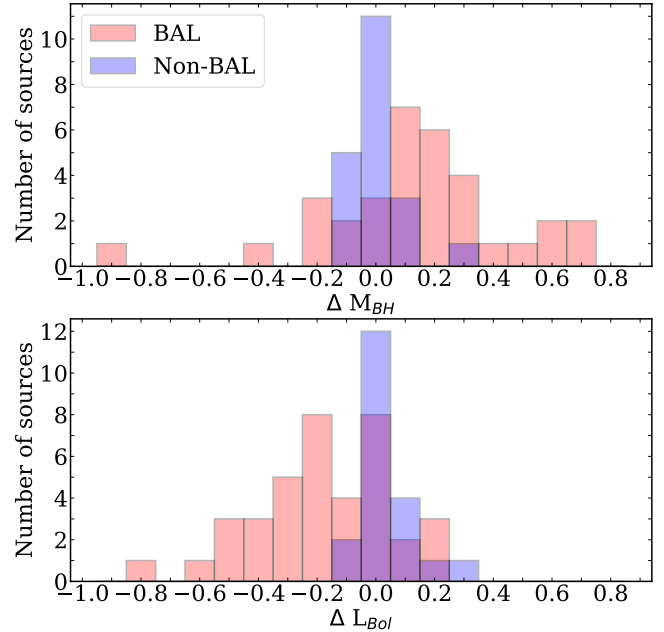


Figure A1. In this figure, we show the distribution of differences in the estimated values of M_{BH} (ΔM_{BH}) and L_{bol} (ΔL_{Bol}) between Shen et al. (2011) and this study for 38 UFO BAL sources and 20 non-BAL sources from the control sample.

to overestimation C IV BEL FWHM and underestimation of L_{1350} which leads to similar problems in the calculation of M_{BH} and L_{bol} respectively. Hence, we did a detailed visual inspection to select line-free regions for each source in our sample and used PyQSOFit to calculate the quasar properties mentioned above.

APPENDIX B: UFO BAL SAMPLE

This paper has been typeset from a $\text{\TeX}/\text{\LaTeX}$ file prepared by the author.

Table B1. Log of sources, observations, details of spectra obtained at different epochs

QSO	Telescope	Date (M/D/Y)	MJD	Exposure time (s)	Wavelength range (Å)	Spectral res. (km s ⁻¹)	S/N ^b
J002809.45-053941.6	SDSS	10-06-2013	56571	4500	3562-10341	150	16.52
	SALT	07-21-2020	59051	2400	4461-7524	304	33.54
	SALT	06-20-2021	59385	2400	3321-6430	304	5.01
	SALT	06-08-2022	59738	2400	3312-6426	304	22.42
J003419.19+030913.1	SDSS	12-01-2010	55531	3603	3589-10363	150	19.46
	SDSS	11-20-2017	58077	4500	3596-10329	150	20.87
	SALT	07-16-2020	59046	2400	4178-7252	304	35.7
	SALT	07-06-2021	59401	2450	3189-6296	304	36.43
J004613.54+010425.7	SDSS	09-07-2000	51794	3600	3802-9193	150	19.26
	SDSS	10-17-2001	52199	3602	3801-9215	150	23.67
	SDSS	12-21-2009	55186	5402	3578-10353	150	27.49
	SDSS	01-05-2010	55201	7201	3587-10360	150	33.76
	SDSS	09-12-2010	55451	5404	3590-10396	150	31.61
	SALT	06-20-2015	57193	1800	3467-6566	304	19.34
	SALT	07-27-2015	57230	1800	3462-6564	304	38.89
	SDSS	09-13-2015	57278	4500	3576-10334	150	28.48
	SALT	09-16-2015	57281	1800	3471-6566	304	55.92
	SDSS	12-09-2017	58096	4500	3587-10360	150	17.12
	SALT	08-18-2018	58348	1300	3464-6567	304	41.93
	SALT	07-04-2019	58668	1350	3466-6569	304	34.61
	SALT	08-01-2021	59427	1913	3482-6568	304	24.91
J005251.81+090945.2	SDSS	10-21-2011	55855	2702	3557-10346	150	14.08
	SALT	07-16-2020	59046	2300	4601-7655	304	28.96
	SALT	08-03-2021	59429	2300	3468-6566	304	12.12
J005419.98+002727.9	SDSS	09-25-2000	51812	4500	3787-9191	150	14.97
	SDSS	11-28-2000	51876	5100	3808-9215	150	14.02
	SDSS	01-04-2001	51913	13500	3806-9212	150	25.89
	SDSS	11-30-2008	54800	10203	3800-9202	150	23.17
	SDSS	10-12-2010	55481	4504	3591-10401	150	24.01
	SDSS	09-14-2015	57279	4500	3620-10392	150	25.74
	SDSS	12-09-2017	58096	4500	3598-10332	150	18.12
	SALT	08-30-2021	59456	2230	3475-6571	304	23.8
	J013802.07+012424.4	SDSS	11-01-2010	55501	5405	3566-10327	150
SDSS		01-07-2018	58125	3600	3583-10363	150	20.37
SALT		09-20-2020	59112	2150	4464-7526	304	42.59
SALT		08-02-2021	59428	2400	3484-6568	304	40.98
J015244.15+092950.1	SDSS	01-03-2011	55564	6305	3552-10303	150	31.54
	SALT	07-28-2020	59058	2300	3896-6979	304	42.53
	SALT	08-03-2021	59429	2300	3339-6433	304	28.74
	SALT	09-16-2022	59838	2300	3356-6479	304	11.3
J020006.31-003709.7	SDSS	11-23-2000	51871	2700	3805-9204	150	16.96
	SDSS	11-04-2005	53678	6900	3804-9200	150	26.52
	SDSS	01-13-2008	54478	12005	3801-9176	150	30.83
	SDSS	09-10-2010	55449	5404	3566-10322	150	25.73
	SDSS	11-26-2014	56987	6300	3565-10337	150	26.06
	SDSS	11-23-2017	58080	3600	3597-10327	150	24.53
	SALT	09-29-2021	59486	2400	3895-6979	304	29.81
J021606.40+011509.5	SDSS	09-29-2000	51816	2700	3795-9183	150	11.44
	SDSS	10-15-2010	55484	3603	3567-10329	150	22.52
	SDSS	01-21-2015	57043	5400	3566-10337	150	20.75
	SDSS	12-12-2017	58099	5400	3598-10334	150	19.67
	SALT	08-30-2021	59456	2400	4038-7114	304	26.49
	SALT	08-27-2022	59818	2450	4037-7111	304	27.37
J022036.27-081242.9	SDSS	09-10-2001	52162	4501	3806-9204	150	18.3
	SDSS	12-21-2008	54821	10801	3805-9215	150	31.86
	SDSS	09-29-2011	55833	5405	3591-10387	150	25.65

QSO	Telescope	Date (M/D/Y)	MJD	Exposure time (s)	Wavelength range (Å)	Spectral res. (km s ⁻¹)	S/N ^b
	SALT	09-12-2021	59469	2400	3613-6706	304	37.2
	SALT	09-27-2022	59849	2400	3603-6703	304	48.38
J022431.59-052818.9	SDSS	10-17-2012	56217	4504	3561-10332	150	38.56
	SALT	08-07-2021	59433	2200	3755-6843	304	73.21
	SALT	08-21-2022	59812	2200	3754-6841	304	62.41
J022943.90-003458.0	SDSS	12-14-2009	55179	9903	3553-10308	150	29.72
	SDSS	12-16-2009	55181	7204	3561-10322	150	23.62
	SDSS	01-12-2010	55208	14406	3558-10325	150	25.84
	SDSS	02-14-2010	55241	7203	3565-10322	150	26.23
	SDSS	09-06-2010	55445	5404	3566-10334	150	31.12
	SDSS	10-07-2010	55476	7206	3568-10327	150	22.84
	SDSS	09-23-2011	55827	6305	3555-10344	150	25.25
	SDSS	10-22-2011	55856	3603	3553-10346	150	27.5
	SDSS	01-19-2012	55945	6305	3554-10344	150	24.52
	SDSS	10-19-2012	56219	5404	3565-10344	150	27.09
	SDSS	10-19-2012	56219	4504	3566-10344	150	23.27
	SDSS	09-09-2013	56544	7200	3566-10351	150	33.63
	SDSS	10-03-2013	56568	2700	3566-10351	150	19.72
	SDSS	10-31-2013	56596	6300	3563-10349	150	22.46
	SDSS	12-09-2017	58096	4500	3597-10329	150	21.66
J024221.87+004912.7	SDSS	10-04-2000	51821	3600	3797-9183	150	18.13
	SDSS	09-25-2001	52177	3601	3823-9215	150	17.67
	SDSS	10-17-2001	52199	2701	3820-9202	150	16.83
	SDSS	02-20-2010	55247	6301	3580-10346	150	30.25
	SDSS	09-16-2010	55455	4504	3594-10380	150	27.16
	SDSS	09-14-2015	57279	2700	3576-10334	150	21.93
	SDSS	01-05-2017	57758	2700	3572-10334	150	10.89
	SDSS	11-16-2017	58073	5400	3598-10325	150	27.23
	SALT	09-11-2021	59468	2400	3757-6844	304	50.11
J024457.18-010809.8	SDSS	11-23-2000	51871	2700	3818-9189	150	10.82
	SDSS	02-20-2010	55247	6301	3564-10318	150	19.6
	SDSS	09-16-2010	55455	4504	3566-10337	150	10.53
	SDSS	01-19-2015	57041	7200	3568-10337	150	19.15
	SDSS	12-21-2016	57743	5400	3604-10334	150	20.96
	SALT	09-07-2022	59829	2400	5863-8855	304	19.21
J081417.55-000455.0	SDSS	03-22-2006	53816	6900	3801-9191	150	19.04
	SDSS	11-24-2011	55889	3603	3558-10346	150	24.15
	SALT	12-25-2020	59208	2500	3474-6572	304	59.11
	SALT	12-31-2021	59579	2500	3465-6568	304	48.11
J081737.08+071723.9	SDSS	11-30-2011	55895	5405	3582-10356	150	26.86
	SALT	12-23-2020	59206	2400	3311-6421	304	83.16
J083126.15+035408.1	SDSS	01-07-2003	52646	4200	3817-9183	150	15.31
	SDSS	03-26-2011	55646	4504	3551-10337	150	23.78
	SALT	01-07-2022	59586	2400	3754-6842	304	29.06
J083745.74+052109.4	SDSS	03-10-2003	52708	2400	3796-9189	150	15.22
	SDSS	01-01-2012	55927	2702	3560-10346	150	19.78
	SALT	02-19-2021	59264	2400	4180-7252	304	58.73
J084502.73+081214.2	SDSS	11-21-2003	52964	2240	3808-9227	150	12.19
	SDSS	11-28-2011	55893	7206	3581-10384	150	28.26
	SDSS	01-20-2012	55946	3603	3604-10365	150	22.3
J091127.61+055054.1	SDSS	01-13-2003	52652	3150	3804-9215	150	25.41
	SDSS	12-01-2011	55896	3603	3557-10332	150	22.52
	SALT	03-29-2016	57476	1900	4554-6602	304	28.18
J092437.70-012844.2	SDSS	02-16-2010	55243	9001	3583-10358	150	32.02
	SALT	12-25-2020	59208	2400	3285-6428	304	43.77

QSO	Telescope	Date (M/D/Y)	MJD	Exposure time (s)	Wavelength range (Å)	Spectral res. (km s ⁻¹)	S/N ^b
J093251.98+023727.0	SDSS	02-25-2001	51965	4505	3815-9202	150	17.15
	SDSS	04-09-2011	55660	7206	3593-10392	150	28.69
	SALT	02-23-2021	59268	2400	3890-6684	304	34.29
	SALT	01-01-2022	59580	2400	3896-6979	304	47.79
J095132.13-015706.9	SDSS	01-03-2011	55564	5405	3555-10315	150	11.62
	SALT	01-15-2021	59229	2500	4320-7384	304	42.17
	SALT	02-23-2022	59633	2600	4319-7385	304	35.46
J100653.26+011938.7	SDSS	03-30-2011	55650	4504	3551-10308	150	24.81
	SALT	01-12-2021	59226	2500	2906-6215	304	42.49
J100716.69+030438.7	SDSS	11-22-2001	52235	4502	3822-9208	150	24.88
	SDSS	02-26-2009	54888	9304	3808-9212	150	27.91
	SDSS	03-30-2011	55650	4504	3595-10389	150	23.0
	SALT	02-05-2016	57423	2125	4171-6239	304	32.33
	SALT	01-31-2020	58879	1250	4167-6245	304	28.48
	SALT	01-07-2021	59221	2400	3897-6979	304	32.49
J105454.51+015008.4	SDSS	03-20-2002	52353	2702	3801-9206	150	12.88
	SDSS	03-28-2011	55648	4504	3557-10322	150	19.51
	SALT	02-03-2021	59248	2600	3031-6153	304	17.96
	SALT	01-28-2022	59607	2600	3014-6152	304	30.83
J111051.75-014002.7	SDSS	02-13-2010	55240	8105	3580-10370	150	25.62
	SDSS	02-19-2010	55246	8103	3584-10370	150	20.17
	SALT	02-04-2021	59249	2400	3758-6843	304	30.94
J111656.89+080829.4	SDSS	04-17-2004	53112	3600	3803-9215	150	20.66
	SDSS	12-11-2012	56272	5405	3610-10387	150	23.62
J113509.02-024015.8	SDSS	01-11-2010	55207	10804	3565-10306	150	22.37
	SALT	01-18-2021	59232	2400	3322-6425	304	44.93
	SALT	01-09-2022	59588	2400	3331-6479	304	33.94
J114319.15+091226.5	SDSS	02-23-2012	55980	4504	3553-10341	150	17.0
	SALT	02-06-2021	59251	2350	3172-6286	304	26.1
J115636.82+085628.9	SDSS	04-04-2003	52733	2340	3808-9212	150	11.27
	SDSS	02-03-2012	55960	3603	3555-10344	150	17.59
	SALT	04-21-2022	59690	2350	3897-6980	304	16.79
J120508.10+013455.8	SDSS	04-25-2001	52024	5403	3811-9193	150	16.99
	SDSS	03-11-2011	55631	4504	3555-10327	150	31.11
	SALT	03-13-2016	57460	2100	4365-6423	304	27.8
	SALT	02-05-2020	58884	1200	4073-6154	304	21.72
	SALT	02-08-2021	59253	2400	3898-6979	304	43.21
J120819.29+035559.4	SDSS	04-12-2002	52376	2701	3816-9215	150	15.04
	SDSS	03-13-2011	55633	7206	3561-10327	150	25.58
	SALT	02-04-2021	59249	2500	3754-6841	304	11.97
J121549.81-003432.1	SDSS	04-01-2001	52000	3602	3815-9191	150	30.61
	SDSS	05-11-2010	55327	8107	3564-10315	150	29.43
	SALT	01-28-2022	59607	2400	3611-6705	304	60.09
J130116.33+031425.7	SDSS	04-28-2001	52027	3602	3827-9215	150	15.17
	SDSS	05-01-2011	55682	4504	3557-10332	150	10.58
	SALT	04-22-2022	59691	2300	3896-6979	304	25.4
J131714.22+010013.1	SDSS	02-04-2000	51578	2700	3802-9206	150	12.69
	SDSS	05-01-2000	51665	3600	3830-9212	150	11.23
	SDSS	03-16-2001	51984	3602	3823-9215	150	18.63
	SDSS	05-05-2010	55321	3603	3585-10392	150	24.31
	SDSS	05-12-2010	55328	6305	3564-10310	150	22.51
	SALT	04-21-2022	59690	2400	4745-7791	304	20.01

QSO	Telescope	Date (M/D/Y)	MJD	Exposure time (s)	Wavelength range (Å)	Spectral res. (km s ⁻¹)	S/N ^b
J133138.49+004221.1	SDSS	04-28-2000	51662	2700	3813-9234	150	9.03
	SDSS	02-15-2001	51955	6300	3811-9215	150	12.53
	SDSS	02-13-2011	55605	3603	3595-10363	150	12.1
	SDSS	03-02-2011	55622	4504	3557-10320	150	10.73
J134112.37-011545.6	SDSS	06-02-2002	52427	3003	3816-9212	150	18.34
	SDSS	03-10-2011	55630	3603	3558-10327	150	18.49
	SALT	04-23-2021	59327	2307	3612-6705	304	33.64
J134320.72+035148.5	SDSS	04-08-2011	55659	3603	3558-10332	150	17.71
	SALT	03-07-2021	59280	2400	3898-6980	304	50.5
	SALT	02-23-2022	59633	2400	3897-6979	304	26.76
J135031.73+084354.7	SDSS	02-21-2012	55978	3603	3605-10392	150	22.74
	SALT	04-02-2021	59306	2300	3617-6708	304	6.51
	SALT	02-24-2022	59634	2350	3613-6705	304	19.63
J135721.77+005501.1	SDSS	04-07-2000	51641	3600	3802-9215	150	17.21
	SDSS	02-02-2001	51942	3600	3812-9234	150	19.8
	SDSS	03-11-2011	55631	4504	3594-10394	150	29.29
	SALT	02-07-2022	59617	2400	3610-6705	304	34.08
J135955.65+031025.9	SDSS	04-26-2011	55677	7206	3556-10329	150	19.09
	SALT	03-25-2021	59298	2400	3612-6707	304	48.81
J140053.02+050708.8	SDSS	04-26-2011	55677	7206	3593-10392	150	19.41
	SALT	05-14-2020	58983	2400	4178-7253	304	23.91
	SALT	05-02-2021	59336	2400	3036-6159	304	24.8
J140532.90+022957.3	SDSS	03-25-2001	51993	2702	3801-9219	150	16.06
	SDSS	05-16-2010	55332	3603	3590-10389	150	21.12
	SALT	05-19-2021	59353	2400	3751-6842	304	42.15
	SALT	05-05-2022	59704	2450	3757-6847	304	55.47
J142405.57+044105.5	SDSS	04-02-2011	55653	2702	3597-10392	150	23.39
	SALT	05-23-2020	58992	2400	4037-7117	304	56.26
	SALT	05-03-2021	59337	2400	3046-6162	304	52.1
	SALT	05-05-2022	59704	2450	3038-6152	304	54.02
J144514.86-002358.1	SDSS	06-09-2008	54626	14504	3809-9179	150	48.75
	SDSS	07-06-2008	54653	13506	3808-9176	150	31.09
	SDSS	06-05-2010	55352	5404	3574-10313	150	35.13
	SALT	06-19-2021	59384	2400	4039-7115	304	58.95
J145229.08+093204.9	SDSS	04-02-2006	53827	4900	3808-9204	150	15.0
	SDSS	02-29-2012	55986	3603	3599-10389	150	19.78
	SALT	04-04-2021	59308	2300	3315-6426	304	39.04
	SALT	05-04-2022	59703	2320	3304-6425	304	40.49
J150033.53+003353.6	SDSS	03-13-2000	51616	1800	3805-9212	150	12.86
	SDSS	03-22-2001	51990	2701	3811-9219	150	12.92
	SDSS	03-12-2011	55632	5405	3595-10353	150	26.79
	SALT	05-13-2019	58616	1300	4323-7385	304	30.06
	SALT	07-22-2020	59052	2300	4324-7385	304	47.61
	SALT	08-03-2021	59429	2300	4324-7386	304	40.08
J154757.71+060626.6	SDSS	06-11-2004	53167	3300	3799-9204	150	26.15
	SDSS	05-26-2011	55707	3603	3595-10387	150	34.12
	SALT	05-14-2021	59348	2200	3748-6842	304	83.34
J160622.00+071849.9	SDSS	05-08-2005	53498	3000	3817-9189	150	14.54
	SDSS	04-01-2012	56018	2702	3564-10341	150	20.25
	SALT	05-28-2020	58997	2400	3754-6842	304	28.99
	SALT	06-19-2021	59384	2400	3315-6430	304	19.91

QSO	Telescope	Date (M/D/Y)	MJD	Exposure time (s)	Wavelength range (Å)	Spectral res. (km s ⁻¹)	S/N ^b
J160650.08+074648.7	SDSS	04-01-2012	56018	2702	3564-10339	150	20.98
	SALT	06-26-2020	59026	2300	4321-7389	304	36.35
	SALT	06-20-2021	59385	2300	3198-6294	304	20.44
J160956.17+052651.2	SDSS	08-15-2007	54327	11111	3817-9200	150	22.47
	SDSS	05-27-2011	55708	4504	3560-10322	150	17.41
	SALT	06-02-2020	59002	2400	4321-7389	304	8.51
	SALT	05-12-2021	59346	2400	3163-6288	304	33.35
J162122.54+075808.4	SDSS	05-11-2005	53501	4200	3808-9215	150	19.81
	SDSS	03-30-2012	56016	4504	3557-10349	150	29.21
	SALT	06-08-2015	57181	2000	4046-7109	304	32.23
	SALT	05-07-2018	58245	1150	4041-7114	304	14.71
	SALT	05-03-2019	58606	1150	4038-7110	304	22.32
	SALT	05-22-2020	58991	2172	4038-7117	304	36.68
	SALT	05-10-2021	59344	2300	3326-6423	304	61.44
	SALT	06-03-2022	59733	2300	3301-6423	304	48.19
	SALT	06-26-2022	59756	2300	3303-6424	304	46.3
J212635.35-021119.3	SDSS	11-16-2011	55881	6305	3556-10339	150	20.73
	SALT	05-18-2020	58987	2400	4321-7389	304	33.36
	SALT	05-09-2021	59343	2400	3306-6425	304	44.39
	SALT	05-12-2022	59711	2400	3302-6426	304	38.2
J213054.48+011500.5	SDSS	11-02-2003	52945	7500	3803-9204	150	24.37
	SDSS	09-24-2011	55828	4504	3592-10349	150	35.55
	SDSS	09-25-2011	55829	4504	3555-10341	150	20.17
	SDSS	06-28-2017	57932	4500	3615-10341	150	29.49
	SDSS	10-14-2017	58040	3600	3600-10329	150	30.77
	SALT	06-13-2018	58282	1200	3616-6702	304	34.03
	SALT	06-09-2019	58643	1200	3613-6703	304	40.73
	SALT	06-19-2020	59019	2400	3611-6706	304	56.29
	SALT	06-04-2021	59369	2300	3617-6704	304	58.58
J213758.95+084433.2	SDSS	09-12-2010	55451	5404	3590-10396	150	28.47
	SALT	05-21-2020	58990	2300	4040-7118	304	26.87
	SALT	06-03-2020	59003	2350	3475-6569	304	16.53
	SALT	06-11-2021	59376	2300	3478-6569	304	53.47
	SALT	06-02-2022	59732	2300	4039-7113	304	43.56
J220911.22-012643.7	SDSS	09-24-2011	55828	6305	3595-10360	150	25.26
	SDSS	10-11-2017	58037	4500	3596-10332	150	22.43
	SDSS	10-16-2017	58042	5400	3599-10327	150	23.66
	SALT	05-31-2020	59000	2400	4322-7387	304	37.44
	SALT	06-06-2021	59371	2400	3196-6292	304	34.84
J222157.97-010331.1	SDSS	11-28-2003	52971	8400	3796-9202	150	24.26
	SDSS	09-04-2010	55443	4504	3558-10325	150	28.81
	SDSS	09-17-2017	58013	3600	3594-10334	150	29.07
	SDSS	10-12-2017	58038	5400	3599-10327	150	30.45
	SALT	07-22-2020	59052	2400	4743-7791	304	64.59
	SALT	06-11-2021	59376	2400	3474-6570	304	50.32
J223934.45-004707.2	SDSS	08-24-2001	52145	2701	3801-9202	150	17.2
	SDSS	10-01-2010	55470	6305	3564-10327	150	27.68
	SDSS	12-02-2016	57724	4500	3607-10334	150	27.1
	SDSS	10-17-2017	58043	3600	3593-10356	150	30.01
	SALT	10-12-2020	59134	2300	4037-7117	304	37.27
	SALT	07-19-2021	59414	2300	4036-7116	304	39.71
J225608.48+010557.8	SDSS	09-22-2001	52174	949	3820-9206	150	5.76
	SDSS	09-26-2001	52178	5405	3819-9204	150	16.36
	SDSS	10-02-2010	55471	7206	3590-10396	150	29.93
	SDSS	09-19-2017	58015	4500	3595-10334	150	27.99
	SALT	07-17-2021	59412	2400	4037-7115	304	36.48

a

QSO	Telescope	Date (M/D/Y)	MJD	Exposure time (s)	Wavelength range (Å)	Spectral res. (km s ⁻¹)	S/N ^b
J231027.23+074658.2	SDSS	09-17-2012	56187	4504	3611-10392	150	23.26
	SALT	07-25-2020	59055	2300	4178-7252	304	28.78
	SALT	07-18-2021	59413	2300	3175-6290	304	37.9
	SALT	06-27-2022	59757	2300	3160-6283	304	29.01
J235238.08+010552.3	SDSS	09-01-2000	51788	1800	3794-9196	150	19.94
	SDSS	10-02-2010	55471	7206	3595-10387	150	35.06
	SDSS	10-29-2014	56959	12601	3609-10392	150	65.06
	SDSS	10-21-2016	57682	7200	3571-10332	150	37.48
	SDSS	11-21-2016	57713	6300	3609-10334	150	42.64
	SDSS	11-24-2017	58081	4500	3598-10332	150	34.49
	SALT	06-19-2021	59384	2400	3613-6706	304	62.33
	SALT	06-26-2022	59756	2400	3615-6705	304	54.81
J235507.36-035709.6	SDSS	09-30-2013	56565	3600	3611-10387	150	17.51
	SALT	07-29-2020	59059	2400	4463-7523	304	37.82
	SALT	07-07-2021	59402	2400	3305-6432	304	59.01
J132216.25+052446.3	SDSS	04-12-2002	52376	2402	3822-9202	150	13.34
	SDSS	03-13-2011	55633	7206	3595-10394	150	26.43
	SDSS	05-22-2011	55703	4504	3559-10329	150	26.11
	SALT	06-21-2015	57194	2400	3210-6290	304	29.47
	SALT	04-15-2016	57493	2400	3136-6282	304	22.87
	SALT	05-07-2018	58245	2000	3166-6284	304	15.62
	SALT	06-09-2019	58643	2400	3172-6284	304	19.94
	SALT	03-23-2020	58931	1200	3177-6290	304	35.68
	SALT	02-17-2021	59262	2500	3171-6291	304	42.37
	SALT	05-10-2021	59344	2500	3177-6290	304	53.46
	SALT	06-02-2022	59732	2500	3184-6294	304	47.61
	SALT	06-04-2022	59734	2500	3191-6292	304	39.67

a

b

Table B2. BAL properties at different epochs

QSO	z_{em}	BAL	z_{abs}	v_{min} km s^{-1}	v_{max} km s^{-1}	MJD	v_{cent} km s^{-1}	W \AA	σ_W \AA	d_{BAL}						
J0028-0539	2.5584	1	2.36	10378	25096	56571	17001	25.29	0.25	0.66						
						59051	16302	19.93	0.13	0.57						
						59738	16333	25.47	0.19	0.66						
J0034+0309	2.3329	1	2.14	10799	26307	55531	17575	19.30	0.23	0.59						
						58077	16669	27.14	0.22	0.71						
						59046	16659	25.65	0.14	0.65						
						59401	16683	23.98	0.13	0.59						
J0046+0104	2.1492	1	2.01	10202	19450	51794	13962	25.19	0.17	0.95						
						52199	14025	23.74	0.13	0.90						
						55186	13761	22.90	0.12	0.91						
						55201	13816	23.25	0.08	0.90						
						55451	13782	24.04	0.09	0.92						
						57193	13689	21.15	0.17	0.95						
						57230	13786	21.26	0.08	0.88						
						57278	13823	22.61	0.10	0.90						
						57281	13752	21.61	0.05	0.88						
						58096	13730	23.16	0.19	0.91						
						58348	13615	20.73	0.07	0.90						
J0052+0909	2.6625	1	2.43	10672	30000	55855	19516	48.13	0.30	0.82						
						59046	19161	42.99	0.18	0.76						
						59429	19035	40.52	0.43	0.78						
						J0054+0027	2.5142	1	2.42	4426	11048	51812	8205	7.65	0.19	0.42
												51876	8137	6.55	0.19	0.36
												51913	8304	6.36	0.11	0.32
												54800	7132	7.72	0.11	0.44
												55481	7239	8.99	0.11	0.49
												57279	7446	8.85	0.10	0.45
												58096	7439	7.93	0.14	0.38
												59456	7477	8.90	0.12	0.53
J0138+0124	2.5441	1	2.42	3000	28896							51812	18192	11.21	0.27	0.38
												51876	18549	12.08	0.27	0.42
												51913	18146	11.24	0.16	0.36
						54800	18838	11.37	0.17	0.37						
						55481	18729	11.65	0.16	0.42						
						57279	18625	10.30	0.16	0.47						
						58096	18795	11.81	0.22	0.46						
						59456	19159	10.09	0.20	0.46						
						J0152+0929	2.1794	1	2.04	6840	26925	55501	10598	77.95	0.17	0.99
												58125	10917	80.06	0.22	1.00
												59112	10885	81.47	0.12	0.99
59428	11004	80.22	0.14	1.00												
J0200-0037	2.1422	1	1.99	6846	29777	55564	13613	34.36	0.16	0.95						
						59058	12701	33.96	0.13	0.96						
						59429	12078	31.55	0.21	0.98						
J0216+0115	2.2310	1	2.19	3191	6227	51871	14604	59.89	0.35	0.99						
						53678	14745	62.95	0.22	0.99						
						54478	14383	63.06	0.19	1.00						
						55449	14836	65.38	0.22	0.99						
						56987	13973	59.45	0.21	0.99						
						58080	13818	58.57	0.20	1.00						
						59486	14562	64.81	0.20	0.98						
						J0216+0115	2.2310	1	2.19	3191	6227	51816	4236	7.68	0.19	0.99
												55484	4151	6.63	0.07	0.93
												57043	4139	6.36	0.09	0.91
												58099	4110	5.58	0.10	0.87
59456	4242	4.98	0.09	0.69												
59818	4290	6.27	0.07	0.88												
J0216+0115	2.2310	2	2.02	7538	29943							51816	20709	39.28	0.57	0.62
												55484	20200	26.89	0.24	0.49
												57043	20076	22.25	0.30	0.41
												58099	20356	16.64	0.31	0.33
												59456	20265	11.87	0.25	0.24
59818	18961	17.02	0.23	0.30												

QSO	z_{em}	BAL	z_{abs}	v_{min} km s ⁻¹	v_{max} km s ⁻¹	MJD	v_{cent} km s ⁻¹	W Å	σ_W Å	d_{BAL}
J0220-0812	2.0095	1	1.86	9509	29709	52162	15612	29.76	0.39	0.88
						54821	14903	26.78	0.20	0.90
						55833	16113	33.45	0.27	0.88
						59469	15649	31.23	0.15	0.90
						59849	16394	36.82	0.10	0.92
J0224-0528	2.0845	1	1.91	14234	20623	56217	16954	5.28	0.09	0.32
						59433	17024	8.77	0.04	0.56
						59812	16978	9.59	0.05	0.62
		2	1.85	22059	27995	56217	24036	1.21	0.09	0.09
						59433	25110	4.77	0.04	0.22
				59812	25143	4.44	0.05	0.25		
J0229-0034	2.1382	1	2.03	3083	28332	55179	10407	69.47	0.16	1.00
						55181	10547	68.81	0.21	1.00
						55208	10490	69.11	0.20	0.99
						55241	10678	71.22	0.18	1.00
						55445	10539	70.67	0.16	0.99
						55476	10579	68.78	0.22	0.99
						55827	10439	68.39	0.20	1.00
						55856	10399	69.25	0.18	0.99
						55945	10048	67.27	0.20	1.00
						56219	10150	66.26	0.23	1.00
						56544	10032	65.81	0.15	1.00
						56568	10146	67.26	0.25	1.00
						56596	10525	68.45	0.23	0.99
						58096	9641	60.48	0.26	1.00
						J0242+0049	2.0573	1	1.88	10573
52177	18117	21.33	0.31	0.72						
52199	17851	18.79	0.34	0.70						
55247	18345	13.49	0.20	0.42						
55455	18464	14.74	0.18	0.46						
57279	19202	7.88	0.23	0.23						
57758	18655	8.62	0.51	0.28						
58073	19653	7.38	0.18	0.22						
59468	19678	12.92	0.10	0.29						
51871	18923	31.77	0.37	0.74						
J0244-0108	3.9856	1	3.68	10283	27536	55247	18561	27.77	0.22	0.69
						55455	18532	28.37	0.43	0.69
						57041	18489	28.17	0.24	0.70
						57743	18555	28.94	0.22	0.71
						59829	18355	24.53	0.19	0.70
J0814-0004	2.5936	1	2.37	10636	29162	53816	19132	16.37	0.26	0.38
						55889	18559	18.23	0.19	0.47
						59208	21345	21.27	0.10	0.45
						59579	21479	20.97	0.11	0.41
J0817+0717	2.4428	1	2.33	4641	18133	55895	9764	33.87	0.12	0.87
						59206	9648	33.50	0.04	0.85
J0831+0354	2.0761	1	1.95	8823	27670	52646	12221	17.18	0.38	0.84
						55646	13555	25.44	0.22	0.83
						59586	15908	37.80	0.18	0.81
J0837+0521	2.3624	1	2.31	3000	7547	52708	4763	9.04	0.11	0.71
						55927	4717	9.82	0.08	0.79
						59264	4611	6.03	0.03	0.58
		2	2.10	22073	28994	52708	24320	5.34	0.25	0.57
						55927	24962	9.75	0.15	0.57
						59264	24713	3.19	0.06	0.26
J0845+0812	2.3545	1	2.13	15183	27269	52964	20958	22.29	0.35	0.64
						55893	21724	20.24	0.13	0.62
						55946	21841	17.99	0.18	0.61
J0911+0550	2.7933	1	2.58	12300	21914	52652	17160	11.88	0.20	0.65
						55896	16466	10.21	0.23	0.66
						57476	14083	2.39	0.12	0.65
						55243	5701	9.35	0.04	0.95
J0924-0128	2.4461	1	2.38	4427	7118	59208	5719	9.20	0.04	0.94
						55243	20066	22.18	0.16	0.70
		2	2.22	9527	28598	59208	20156	29.38	0.13	0.55

QSO	z_{em}	BAL	z_{abs}	v_{min} km s ⁻¹	v_{max} km s ⁻¹	MJD	v_{cent} km s ⁻¹	W Å	σ_W Å	d_{BAL}				
J0932+0237	2.1679	1	1.96	13042	30000	51965	20678	33.00	0.34	0.81				
						55660	21275	38.93	0.20	0.80				
						59268	21801	37.14	0.18	0.78				
						59580	21676	42.90	0.10	0.79				
J0951-0157	3.2553	1	2.97	14909	27271	55564	20964	23.18	0.38	0.82				
						59229	20496	13.38	0.07	0.70				
						59633	20472	12.39	0.10	0.70				
J1006+0119	2.3030	1	2.16	6674	24194	55650	13439	38.84	0.17	0.86				
						59226	14512	47.39	0.11	0.86				
J1007+0304	2.1245	1	1.92	15770	24885	52235	20501	8.73	0.16	0.60				
						54888	19799	13.06	0.14	0.68				
						55650	19608	10.78	0.17	0.62				
						57423	19813	10.14	0.09	0.52				
						58879	19732	5.65	0.12	0.36				
J1054+0150	2.2366	1	2.08	13434	17152	52353	14956	6.29	0.19	0.60				
						55648	15174	10.57	0.11	0.81				
						59248	15088	5.47	0.14	0.67				
						59607	15205	6.92	0.07	0.68				
						52353	21241	1.24	0.23	0.18				
		2	2.01	19284	23542	55648	21168	5.44	0.14	0.45				
						59248	21813	0.98	0.15	0.16				
						59607	21308	0.89	0.08	0.14				
						55240	15381	37.93	0.54	0.82				
						55246	15300	38.05	1.55	0.83				
J1110-0140	2.8192	1	2.63	8252	24514	59249	15690	35.48	0.18	0.80				
						53112	19949	6.74	0.18	0.28				
						56272	19671	6.45	0.17	0.34				
J1116+0808	3.2429	1	2.97	16170	24210	55207	21098	9.11	0.16	0.44				
						59232	20291	10.43	0.08	0.45				
						59588	20122	6.97	0.10	0.27				
J1135-0240	2.4611	1	2.23	15141	25096	55980	11928	21.56	0.21	0.75				
						59251	12014	22.30	0.14	0.80				
J1143+0912	2.3253	1	2.20	5665	16556	52733	17105	47.75	0.59	0.77				
						55960	18849	66.07	0.28	0.79				
						59690	16210	30.72	0.35	0.60				
J1156+0856	2.1077	1	1.94	6919	30000	52024	19145	35.06	0.32	0.83				
						55631	18974	20.69	0.16	0.61				
						57460	17635	12.95	0.15	0.63				
						58884	19444	23.28	0.18	0.70				
						59253	19309	16.07	0.12	0.53				
J1205+0134	2.1523	1	1.96	12909	29458	52376	7127	6.12	0.17	0.63				
						55633	7142	8.04	0.10	0.85				
						59249	7388	8.23	0.24	0.74				
						52376	20805	8.58	0.35	0.43				
						55633	21064	12.22	0.20	0.54				
						59249	19993	18.72	0.40	0.70				
J1208+0355	2.0210	1	1.95	4995	9738	52000	13381	32.34	0.23	0.72				
						55327	13200	33.87	0.43	0.73				
						59607	12894	38.53	0.07	0.71				
						55682	20012	10.88	0.37	0.55				
J1215-0034	2.6987	1	2.54	4151	22790	59691	20812	7.22	0.17	0.35				
						51578	8998	22.47	0.41	0.79				
						51665	9199	24.62	0.71	0.86				
J1301+0314	2.1115	1	1.91	16175	25380	51984	9153	23.70	0.39	0.83				
						55321	9507	33.58	0.33	0.88				
						55328	9500	34.10	0.46	0.88				
						59690	9310	31.26	0.27	0.99				
						51578	20858	1.02	0.25	0.16				
J1317+0100	2.6961	1	2.59	3816	18015	51665	21688	2.10	0.31	0.32				
						51984	21410	2.10	0.20	0.21				
						55321	22418	4.70	0.12	0.25				
						55328	22395	4.50	0.12	0.22				
						59690	22195	4.11	0.18	0.26				
						2	2.45	19596	25568	51578	20858	1.02	0.25	0.16
						51665	21688	2.10	0.31	0.32				

QSO	z_{em}	BAL	z_{abs}	v_{min} km s ⁻¹	v_{max} km s ⁻¹	MJD	v_{cent} km s ⁻¹	W Å	σ_W Å	d_{BAL}
J1331+0042	2.4341	1	2.35	6555	9453	51662	7810	2.11	0.21	0.22
						51955	7931	3.65	0.16	0.39
						55605	7727	3.59	0.15	0.48
						55622	7745	3.29	0.16	0.37
						51662	14261	2.01	0.33	0.24
J1341-0115	2.7682	1	2.55	8502	25835	51955	13900	4.17	0.24	0.32
						55605	14087	4.73	0.24	0.43
						55622	14216	4.74	0.25	0.33
						52427	17748	26.80	0.47	0.90
						55630	17947	32.93	0.78	0.92
J1343+0351	2.8686	1	2.68	12032	19532	59327	17654	39.86	0.16	0.82
						55659	15355	13.37	0.18	0.75
J1350+0843	2.6157	1	2.44	13629	17632	59280	15745	9.42	0.06	0.57
						59633	15651	11.25	0.13	0.60
						55978	15355	6.15	0.09	0.60
J1357+0055	2.0081	1	1.80	11851	30000	59306	15519	5.12	0.35	0.45
						59634	15605	5.19	0.12	0.39
						51641	21018	12.05	0.34	0.78
J1359+0310	2.6778	1	2.52	8662	19833	51942	21938	18.08	0.29	0.79
						55631	22452	20.69	0.19	0.79
						59617	20448	15.07	0.17	0.66
J1400+0507	2.3015	1	2.16	7038	25561	55677	12662	21.67	0.28	0.79
						58983	14469	41.61	0.24	0.84
						59336	13812	34.13	0.28	0.86
J1405+0229	2.8266	1	2.67	6487	24861	51993	12222	30.31	0.55	0.77
						55332	13240	40.45	0.33	0.79
						59353	10850	17.38	0.12	0.77
J1424+0441	2.2762	1	2.05	11006	28320	59704	11181	13.91	0.09	0.73
						55653	21111	21.11	0.20	0.69
						58992	20826	18.18	0.09	0.61
J1445-0023	2.2296	1	2.05	7822	27489	59337	20717	12.88	0.10	0.57
						59704	21068	12.76	0.10	0.60
						54626	17007	45.47	0.10	0.78
J1452+0932	2.4607	1	2.29	5694	28047	54653	17006	45.87	0.18	0.78
						55352	17171	48.70	0.11	0.78
						59384	17596	44.56	0.09	0.75
J1500+0033	2.4394	1	2.23	9914	27649	53827	14832	46.71	0.31	0.81
						55986	15131	48.80	0.23	0.85
						59308	13715	28.33	0.15	0.72
J1547+0606	2.0188	1	1.95	5432	9467	59703	15250	27.57	0.11	0.63
						51616	18577	18.64	0.38	0.69
						51990	18648	28.63	0.38	0.85
J1606+0718	2.0766	1	1.99	3835	22135	55632	18518	20.03	0.18	0.82
						58616	18137	16.61	0.19	0.80
						59052	18386	21.09	0.10	0.81
J1606+0746	2.3687	1	2.20	8414	23723	59429	18430	24.31	0.12	0.87
						53167	7197	13.24	0.07	0.96
						55707	7164	13.23	0.05	0.96
J1609+0526	2.3802	1	2.27	4115	26115	59348	7165	13.76	0.02	0.96
						53167	15460	39.09	0.18	0.89
						55707	15555	40.34	0.12	0.89
J1609+0526	2.3802	1	2.27	4115	26115	59348	15148	38.17	0.04	0.87
						53498	8456	35.48	0.42	1.00
						56018	8323	30.97	0.25	1.00
J1609+0526	2.3802	1	2.27	4115	26115	58997	8890	39.82	0.18	1.00
						59384	8838	38.09	0.32	1.00
						56018	15772	10.58	0.21	0.41
J1609+0526	2.3802	1	2.27	4115	26115	59026	15894	16.37	0.12	0.45
						59385	15383	12.69	0.25	0.43
						54327	9635	38.25	0.24	0.97
J1609+0526	2.3802	1	2.27	4115	26115	55708	11443	53.79	0.28	0.98
						59002	11386	49.43	0.78	0.90
						59346	10841	53.44	0.14	0.98

QSO	z_{em}	BAL	z_{abs}	v_{min} km s ⁻¹	v_{max} km s ⁻¹	MJD	v_{cent} km s ⁻¹	W Å	σ_W Å	d_{BAL}
J1621+0758	2.1394	1	1.98	12355	19811	53501	15544	3.14	0.20	0.19
						56016	15876	8.15	0.12	0.33
						57181	15684	7.32	0.11	0.42
						58245	15757	4.17	0.26	0.26
						58606	16325	4.87	0.14	0.24
						58991	16164	4.20	0.09	0.25
						59344	16472	4.60	0.05	0.20
						59733	16362	4.96	0.07	0.20
						59756	16409	3.16	0.07	0.14
						J2126-0211	2.4629	1	2.23	12298
58987	20283	12.83	0.13	0.46						
59343	20475	14.09	0.09	0.53						
59711	20122	14.16	0.10	0.46						
J2130+0115	2.5275	1	2.26	9697	30000	52945	23298	35.07	0.21	0.70
						55828	22436	33.13	0.12	0.56
						55829	22772	28.03	0.20	0.52
						57932	23203	29.51	0.16	0.58
						58040	23644	23.59	0.16	0.51
						58282	25237	12.11	0.14	0.40
						58643	24679	15.15	0.12	0.44
						59019	24628	15.19	0.08	0.44
J2137+0844	2.1893	1	2.12	4314	9046	55451	6148	15.16	0.07	0.98
						58990	6244	16.19	0.08	1.00
						59003	6248	15.88	0.15	0.99
						59376	6266	15.99	0.04	0.97
						59732	6258	16.47	0.04	0.99
		2	2.05	10082	23576	55451	13630	12.53	0.16	0.60
						58990	14757	25.52	0.16	0.77
						59003	14419	23.14	0.27	0.80
						59376	14149	22.03	0.08	0.75
						59732	14281	23.29	0.09	0.80
J2209-0126	2.4227	1	2.27	5076	30000	55828	13430	66.62	0.17	1.00
						58037	13341	66.13	0.20	1.00
						58042	13272	64.99	0.20	1.00
						59000	13055	61.56	0.13	1.00
						59371	13058	60.93	0.14	1.00
						59732	14281	23.29	0.09	0.80
J2221-0103	2.6754	1	2.44	9723	29032	52971	19427	32.29	0.23	0.76
						55443	20037	20.35	0.16	0.60
						58013	19061	25.65	0.17	0.73
						58038	19010	24.94	0.16	0.72
						59052	18606	15.17	0.08	0.58
						59376	18815	21.66	0.09	0.69
J2239-0047	2.2200	1	2.01	14375	25370	52145	20514	5.90	0.29	0.34
						55470	20072	11.64	0.13	0.36
						57724	20092	5.46	0.18	0.25
						58043	20119	7.24	0.14	0.31
						59134	19827	8.90	0.12	0.35
						59414	19591	8.07	0.11	0.28
J2256+0105	2.2680	1	2.21	3000	8535	52174	5827	15.69	0.45	0.94
						52178	5656	15.96	0.16	0.96
						55471	5672	15.95	0.07	0.93
						58015	5644	15.87	0.07	0.94
						59412	5671	15.21	0.07	0.89
		2	2.05	15840	26759	52174	21107	14.70	0.80	0.57
						52178	21024	11.76	0.33	0.57
						55471	20766	10.47	0.14	0.53
						58015	21010	7.45	0.15	0.51
						59412	20995	14.07	0.12	0.62
J2310+0746	2.3109	1	2.23	6302	9269	56187	7618	7.74	0.08	0.76
						59055	7705	8.65	0.07	0.78
						59413	7751	7.58	0.04	0.70
						59757	7757	8.64	0.05	0.80
		2	2.19	10000	13108	56187	11568	2.17	0.10	0.54
						59055	11584	3.94	0.08	0.62
						59413	11588	1.82	0.05	0.34
						59757	11631	2.66	0.07	0.57

QSO	z_{em}	BAL	z_{abs}	v_{min} km s ⁻¹	v_{max} km s ⁻¹	MJD	v_{cent} km s ⁻¹	W Å	σ_W Å	d_{BAL}						
J2352+0105	2.1513	1	1.92	14600	29706	56187	21494	8.29	0.21	0.30						
						59055	21669	16.88	0.19	0.41						
						59413	21310	5.82	0.11	0.20						
						59757	20810	6.05	0.16	0.29						
						51788	23040	16.74	0.26	0.80						
						55471	23278	15.78	0.15	0.76						
						56959	23028	11.93	0.08	0.70						
						57682	22437	10.18	0.13	0.68						
						57713	22322	10.25	0.12	0.71						
						58081	22575	8.40	0.16	0.70						
J2355-0357	2.4448	1	2.26	11721	28163	59384	23132	13.03	0.07	0.54						
						59756	23354	12.64	0.08	0.57						
						56565	16331	10.48	0.27	0.56						
						59059	17461	11.37	0.12	0.51						
						59402	18210	14.64	0.08	0.48						
						J1322+0524	2.0498	1	1.97	5680	9830	52376	7708	11.49	0.16	0.95
												55633	7591	8.77	0.08	0.82
												55703	7588	8.34	0.08	0.82
												57194	7564	3.59	0.08	0.45
												57493	7546	5.18	0.11	0.56
58245	7639	9.94	0.16	0.89												
58643	7691	11.66	0.11	0.94												
58931	7573	7.56	0.06	0.72												
59262	7629	9.12	0.05	0.87												
59344	7475	6.66	0.04	0.68												
2	1.93	10731	13059	59732	7586			10.42	0.04	0.89						
				59734	7600			9.83	0.05	0.88						
				52376	11980			1.76	0.17	0.25						
				55633	11780			0.69	0.08	0.12						
				55703	11768			0.70	0.08	0.11						
				57194	12089			0.63	0.06	0.11						
				57493	11960			0.85	0.09	0.12						
				58245	12019			1.82	0.13	0.27						
				58643	11931			2.45	0.10	0.29						
				58931	11922			0.86	0.05	0.12						
3	1.85	15600	26632	59262	12034	1.48	0.04	0.20								
				59344	11962	0.81	0.03	0.10								
				59732	11919	1.64	0.04	0.21								
				59734	11944	2.16	0.05	0.26								
				57194	20331	5.95	0.13	0.18								
				57493	20493	7.53	0.17	0.23								
				58245	20483	12.82	0.27	0.45								
				58643	21298	14.03	0.21	0.41								
				58931	20584	6.02	0.11	0.20								
				59262	20787	8.00	0.10	0.25								
59344	20434	5.69	0.07	0.19												
59732	20581	7.47	0.08	0.27												
59734	20685	10.03	0.09	0.31												